PHASE LOCKING OF SOLID-STATE LASER ARRAYS

by

LIPING LIU

A dissertation submitted to the Graduate Faculty in Physics in partial fulfillment of the requirements for the degree of Doctor of Philosophy, the City University of New York

2010

This manuscript has been read and accepted for the Graduate Faculty in Physics in satisfaction of the dissertation requirement for the degree of Doctor of Philosophy.

_____	_____
Date	Chair of Examining Committee Prof. Ying-Chih Chen
_____	_____
Date	Executive Officer Prof. Steven Greenbaum

_____
Prof. Yuhang Ren

_____
Prof. Noel Goddard

_____
Prof. Mark Arend

_____
Prof. Kai Shum

Supervisory Committee

CITY UNIVERSITY OF NEW YORK

ABSTRACT

PHASE LOCKING OF SOLID-STATE LASER ARRAYS

by

LIPING LIU

Adviser: Professor Ying-Chih Chen

This thesis reports a study of phase locking in solid-state laser arrays of a variety of configurations, including a 2x2 Nd:YVO_4 continuous-wave laser array, a two-element passively Q-switched Nd,Cr:YAG laser array, a two-element continuous-wave ytterbium fiber laser array, and a two-element ytterbium fiber lasers passively Q-switched by stimulated Brillouin scattering. Phase locking is accomplished by coupling the lasing elements into a common Fourier-transform resonator, with the lasing elements placed at one focal plane of a converging lens and the output mirror placed at the other focal plane. The control of the relative phase among the elements is done by placing a spatial filter in front of the output mirror to introduce different modal losses. We have succeeded in achieving highly stable phase-locked operation in the in-phase mode in continuous-wave laser arrays. The fringe visibility of the phase-locked beam is nearly 1. As the coupling strength decreases, the transition from phase locked to unlocked mode is abrupt. Phase locking of nano-second pulsed laser arrays requires a tight control of the resonance frequencies and path lengths of the individual lasing elements to ensure the pulses generated by the individual elements to occur simultaneously. As the difference in path lengths increase or the coupling strengths decrease, the transition from the phase

locked to the unlocked states is characterized by a gradual loss of coincidence of the pulses from the individual elements and a reduction in the fringe contrast in the combined laser beam. The current approach of phase locking has high efficiency and is applicable to two-dimensional laser arrays containing a large number of elements.

ACKNOWLEDGEMENTS

I would like to express my deepest and sincerest gratitude to my advisor, Professor Ying-Chih Chen, for his constant guidance, encouragement and patience. His knowledge, experiences and insights in laser physics provided the basis for the work presented in this thesis.

I would like to thank those who have directly helped with the work presented in this thesis. In particular I thank Dr. Yi Zhou and Mr. Fanting Kong for helping doing the experiments together, valuable talks and discussions. I also thank Mr. Richard Krum for machining many precision parts for my experiments and for general advice about making mechanical aspects of our experiments work.

In addition, I am grateful to all the faculty and staff members in the Department of Physics and Astronomy at Hunter College, for support and help, while I was working as a teaching adjunct there.

Finally, my special thanks go to my husband, Jing, for his caring, patience, encouragement and love.

Table of contents:

List of Figures

Chapter 1 Introduction

The first working laser (Ruby laser) was demonstrated by Theodore Mailman in 1960. Since then there has been an intense interest for researchers to develop laser devices that can deliver higher power. High-power lasers are needed for a wide variety of applications, for example, material processing, nonlinear optical processes, remote sensing, fundamental sciences, and laser-induced nuclear fusion. Most of the applications also require high degree of spatial coherence which is needed for focusing the laser beams to a small spot. The maximum available power from a laser is limited by the volume of the gain medium. Increasing the volume of the gain medium, however inevitably faces problems of beam distortion and instability, commonly associated with lasers with a single large cross-sectional area. Combining the output of multiple lasers, each having a smaller volume with a stable laser beam, is a way to achieve high power with good beam quality.

A conceptually simple, although not very attractive example for power scaling would be to tile collimated beams from N independently running lasers side by side. In this way, one may achieve nearly unlimited output power simply by combining the output of a large number of lasers. However, even though the combined power increases in proportion to the number of lasers, the brightness will at most stay at the level of a single laser. Diffraction-limited performance is not possible in this case unless all the lasers operate at the same wavelength and in the same phase so that their fields add coherently in the far field. If all the elements in the laser array operate in the same phase, the total

power is proportional to the number of element and the brightness is proportional to the square of the number of elements.

The objective of this study is to develop an efficient and scalable technique for phase locking of a large number of lasers, including one- and two-dimensional laser arrays operating in the continuous-wave and pulsed mode. Due to increasing importance of fiber lasers in the field of lasers, the technique of phase locking must also adapt to the ever-lasting and random phase fluctuations which are characteristic of all fiber lasers.

Many approaches for phase locking have been proposed and investigated in the past. These include active phase control, evanescent wave coupling, the Talbot resonator, nonlinear coupling, and common-resonator coupling [1].

Active phase control of the phase of the individual elements of laser arrays to maintain a constant relative phase among the elements is most straight forward in concept. This approach has been implemented using the master-oscillator power-amplifier (MOPA) configuration [2-5]. In this approach, the laser beam from the master oscillator is used to seed an array of laser amplifiers. The phase errors of the elements relative to a reference laser beam are individually measured interferometrically and corrected by an array of phase modulators associated with each element. Using high-power, Yb-doped, single-mode amplifiers and lithium niobate phase modulators, Anderegg *et al.* [3] achieved 470 W by coherently combining 4-element fiber array. Shay *et al.* [5] recently demonstrated phase locking of 9 fiber amplifiers using a self-referencing technique that resulted in residual phase error of λ /20. The active control requires individual detection and correction of phase errors of all the elements. The complexity of the setup makes it unpractical for laser arrays with a large number of elements.

Evanescent wave coupling is widely used in gas lasers and semiconductor lasers [7-9]. The coupling is accomplished by placing two or more waveguides in close proximity to one another so that the evanescent waves of the eigenmodes of the individual waveguides overlap with their nearest neighbors. This technique has been applied to laser diode arrays containing tens to hundreds of lasing elements on a single chip, where the coupling is facilitated simply by fabricating the waveguides sufficiently close to one another using microelectronic processing. The technique has also been applied to multi-core optical fibers where the relative phase among the elements is controlled by tailoring the diffraction losses [9,10] and by using the Talbot effect [11,12]. The in-phase operation of an evanescent-coupled multicore fiber laser has been demonstrated. The main challenge is to obtain not only tight coupling, but also reproducible control of the coupling so that all the elements operate in phase rather than out of phase. Evanescent coupling tends to favor the mode with adjacent elements operating with a phase difference of π, which is undesirable for most applications. Furthermore a closely packed 2D laser array will inevitably encounter thermally-induced problems, such as wave front distortion and low efficiency.

Phase locking has also been demonstrated using the Talbot resonator in arrays of semiconductor lasers and solid-state lasers. The Talbot effect is based on the self-imaging effect of coherent periodic structures. The waves from an array of coherent light sources of wavelength λ and periodicity d reproduce the images of the source in the near field after propagating in free space over a distance $Z_T = 2\, d^2 / \lambda$, known as the Talbot distance, or integer multiples of Z_T. (See Fig.1.1) Several groups have demonstrated phase locking in various laser arrays by employing the Talbot resonator [13,14] with a

mirror placed at ½ Z_T to reflect the self-images back to the light sources to facilitate phase locking. No imaging optics is needed. The properties of images at fractional Talbot distances have also been investigated [15-17]. Efficient operation of the Talbot resonator for a linear array requires that the number of elements in the periodic structure be very large. In arrays with a finite number of elements, the Talbot resonator is not efficient because the breakdown of the periodicity near the edges causes the wavefront to curve, which is not easily correctable.

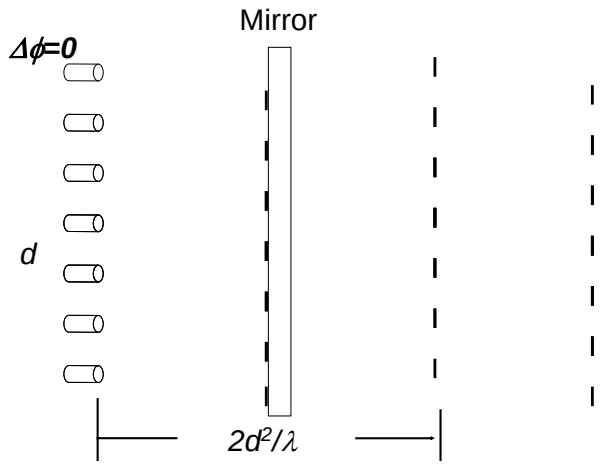

Fig. 1.1 Schematic of Talbot resonator

The Talbot resonator is conceptually simple and elegant. However, like all near-field diffraction effects, the Talbot images involve complicated and rapidly evolving field amplitude and phase, which make the alignment difficult.

A similar self-imaging phenomenon has been found in annular structures with periodicity in the azimuthal direction [11, 12, 15-17]. Phase locking in a two-dimensional fiber laser array containing 18 elements on an annulus has been demonstrated with an annular Talbot resonator [15-17]. Unlike the linear Talbot images which are are exact replica of the sources, the annular Talbot images are much larger in

the radial direction and do not overlap well with the sources. Thus the feedback efficiency of the annular Talbot resonator in free space is low, on the order of 10%, meaning that 90% of the feedback energy is wasted [15]. The beam spreading in the radial direction can be partially corrected by employing an annular waveguide. The theoretical maximum feedback efficiency can be as high as 70 % [17].

Nonlinear optical approaches to beam combining involve phase conjugation and stimulated Brillouin scattering (SBS) or stimulated Raman scattering [18-29]. If the phase conjugate fidelity is high, the effect of wavefront reversal ensures that the Stokes beam propagates back through the laser elements and that the phases of the beams are locked after the second pass through the laser elements. According to Valley *et al.*[18], the first experiments demonstrating phase locking of two channels via SBS were performed by Basov in 1980 using a pulsed laser[19]. Basov split a single beam into two passive channels using a 50/50 beam splitter and coupled both channels into a common waveguide for SBS phase conjugation. The two channels became a single aberrated wavefront in the SBS cell. A high-fidelity, phase-conjugate reflection was created by the SBS cell which phase locked the Stokes beam after back-propagation through the two channels. Many investigations have been performed to coherently combine multiple channels using pulsed lasers in focused SBS cells filled with a liquid or gas.[18, 22-28] The reported experiments were typically successful, combined up to 8 parallel amplifiers[23] and achieved phase errors among the channels as low as λ /27[24]. Another attempt to lock the phases of multiple channels using SBS in a focused cell architecture seeded the SBS cells with a frequency-shifted Stokes seed. This technique has been examined theoretically [27, 29] and experimentally [18, 27], with the goal of fixing a common phase among all the channels through seeding the SBS process. Seeding the SBS process is one method to lower the SBS threshold, but Moyer's results show

that phase conjugation fidelity suffers when this technique is used [27]. Coherent beam combination via SBS has been concentrated in pulsed laser systems due to high SBS threshold. A few of studies used continuous-wave lasers, but none have employed a full spatial phase-conjugate beam. Key issues with nonlinear optical beam combining include scaling to large numbers of elements, having a low threshold, and handling the bandwidth and dynamic range of the required phase corrections.

In the course of studying the techniques of phase locking, we evaluated the applicability of various techniques to laser arrays. The suitable mechanism of phase locking must satisfy the following requirements: (1) The resonator must have high efficiency; (2) The modal pattern must be simple and not critically depending on exact periodicity of the emitters; (3) There must be minimal edge effects in amplitude and phase distribution so that the operation does not need to assume an infinite number of elements in the array; (4) The system can be scaled up to include a large number of elements. We have found that the configuration of coupling a number of lasers to a common Fourier transform resonator, first demonstrated by Menard *et al.* in a two-element system [30], can satisfy the above mentioned requirements and thus adopted this approach.

The schematic of the Fourier transform resonator is shown in Fig 1.2. The lasing elements and the common output mirror are placed at the focal planes of a converging lens. In this arrangement, the electric field at output mirror is the Fourier transform of that of the lasing elements and thus has the same pattern at the beam profile in the far field of the laser array. The beam profiles in the far field are much simpler than those in the near field. For example, the far-field beam profile of a rectangular array is also

rectangular and that of annular array is concentric. A simple spatial filter that matches the intensity minima in the far field can select the operating mode. The simplicity in the mode selection process is a feature that has not been recognized and utilized before.

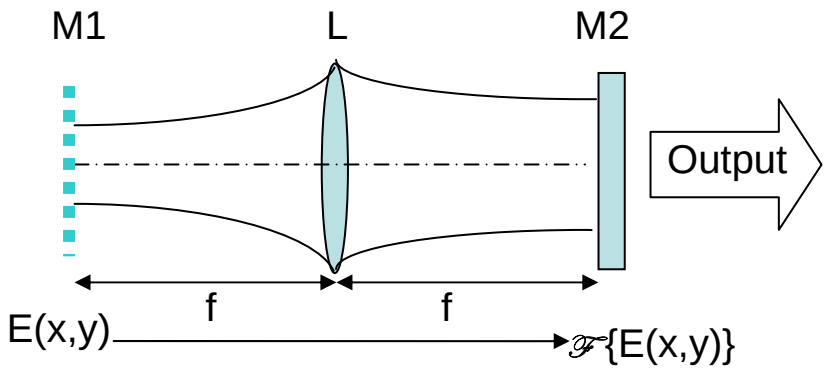

Fig.1.2 Schematic of a self-imaging Fourier Transform resonator

In this thesis, we document the experimental study of phase locking in solid-state lasers. The laser arrays include a two-dimensional 2x2 continuous-wave(CW) neodymium-doped yttrium vanadate laser arrays, a two-element passively Q-switched chromium and neodymium co-doped yttrium aluminum garnet lasers, a continuous-wave two-element ytterbium fiber lasers, and two-element short pulse fiber lasers passively Q-switched by stimulated Brillouin backscattering. Phase locking is accomplished by coupling the gain media to a common Fourier transform resonator, with the array placed at one focal plane of a converging lens and output coupler placed at the other focal plane. Selection of the in-phase mode is accomplished by using a spatial filter placed at the output coupler. For a periodically-spaced laser array, the Fourier-transform resonator provides near 100% efficiency. Compared to the near-field approach, such as the Talbot resonator, phase locking by controlling beam profile in the far field is much simpler and

more efficient. Phase locking of Q-switched lasers has more stringent conditions than CW lasers in terms of the smaller tolerance of frequency detuning between the elements.

This thesis is organized as follows. In Chapter 2, we provide a review of phase locked laser arrays, the supermodes, mode selection and spatial filtering. Chapter 3 describes the physical and optical properties of neodymium-doped solid-state lasers. Chapter 4 provides a brief summary of the spectroscopy of ytterbium-doped silica fiber, and describes the nonlinear effects such as stimulated Brillouin scattering and stimulated Raman scattering. The study of phase locking in solid-state laser array is described in Chapter 5-8. Chapter 5 describes the phase locking of a 2x2 neodymium-doped yttrium vanadate laser array operating in the CW mode, Chapter 6 describes the phase locking of two passively Q-switched pulsed lasers, Chapter 7 describes the phase locking of two ytterbium fiber lasers operating in the CW mode, and Chapter 8 describes the phase locking of two fiber lasers passively Q-switched by stimulated Brillouin scattering. In the end, Chapter 9 provides a summary of the work in this thesis and describes possible areas for further research.

Chapter 2 Laser arrays and phase-locked modes

2.1 Introduction

Laser arrays have become a viable alternative for high-power, good beam quality laser systems. The individual lasers used in the array usually have relatively lower power. When the elements in the laser array are de-coupled, the output is an incoherent superposition of the laser beams of the individual elements. The power density of the output is then proportional to the number of elements. The brightness, defined as the power per unit area per unit solid angle, of the combined output stays the same as the individual elements because the beam area increases while the beam divergence stays constant. If all the elements in the laser array are coherently coupled and operating in the same phase, the resultant beam profile in the far field has a reduced beam divergence which is inversely proportional to the number of elements, and the resultant brightness is proportional to the square of the number of elements

2.2 One-dimensional laser array

The array format has been widely used in semiconductor lasers to achieve high power since 1980s [31]. The coupling between the electric fields of adjacent elements in a semiconductor laser array is typically through the evanescent waves. Two different theories have been used to determine the far-field intensity pattern of phase-locked semiconductor laser array. The coupled mode theory for phase-locked laser arrays was first published by Butler *et al.* [31]. Experiments by Paoli *et al.* [32] and Elper *et al.* [33] confirmed that the theoretical predictions of the coupled-mode theory. The theory shows

that an N-element array has N eigenmodes [36], also called the supermodes whose near-field electric field distribution is given by [37]

$$E_v(y) = \sum_{l=1}^{N} \sin\left(\frac{\pi.mv}{N+1}\right) \exp\left[-\frac{(y_0 - nD)^2}{2\sigma^2}\right] \tag{2.1}$$

Where v is the index of the supermode, m is the element number, N is the total number of elements, n=2m-(N+1) gives the displacement from the end of the array to the m^{th} element, 2D is the spacing between elements, and σ is the Gaussian width of the elements [37].

On the other hand, simple diffraction theory can also be used to analyze the behavior of phase-locked arrays. Scifres *et al.* [38] were the first to analyze a phase-locked laser array using simple diffraction theory. This theory accurately predicts the patterns for supermodes of various phase differences $\Delta\Phi$ between adjacent elements.

The electric field of the semiconductor laser array at the emitting facet can be modeled as a rectified cosine function. Inside the waveguides of the array the electric field is a cosine, and outside the waveguide in the region between elements it is a rapidly decaying exponential function. It is these decaying (evanescent) waves that lead to interaction and phase-locking, but the decaying portion dies off quickly enough that it can be ignored for calculation of the far-field intensity pattern. Therefore, we can approximate the near-field electric field distribution of semiconductor laser array at the emitting facet as:

$$E_{NF}(x) = E(0) \cdot \sum_{n=1}^{N} \cos\left(2\pi \frac{(x - nb)}{2b}\right) \cdot rect\left(\frac{x - nb}{b}\right) \cdot \exp(in\Delta\Phi) \tag{2.2}$$

In this expression, $n=1,\ldots, N$ are the individual elements, x is the distance from the end of the array to the n^{th} element, b is the spacing between elements, and the $\Delta\Phi$ is the phase difference between adjacent elements.

Simple diffraction theory predicts that the far-field electric field distribution of the laser array is proportional to the Fourier transform of the near-field electric field. The intensity in the far field is proportional to $|\mathcal{F}\{E_{NF}(x)\}|^2$, where $\mathcal{F}$ is the Fourier transform operation evaluated at the spatial frequency $f_x \approx \theta/\lambda$, θ is the angular displacement from the center of the array, and λ is the wavelength of the field. Therefore,

$$I(\theta) \propto \left[\sin c\left(f_x b - \frac{1}{2} \right) + \sin c\left(f_x b + \frac{1}{2} \right) \right]^2 \cdot \left[\frac{\sin^2(5\Delta\Phi - 10\pi f_x b)}{\sin^2\left(\frac{\Delta\Phi}{2} - \pi f_x b \right)} \right] \tag{2.3}$$

using the same notation as Equation (2.2). As an example, the near-field and far-field of a 5-parallel-stripe array are shown as in Fig. 2.1.

A close examination of the supermode lateral intensity profiles shows that the highest-order mode has sharp zeros between the elements; and the lowest order mode has nonzero minima. Therefore, the overlap of the intensity profile with the absorbing region is minimal for the highest-order mode. This explains why the highest order supermode tends to be the dominant mode in evanescent coupled laser array.

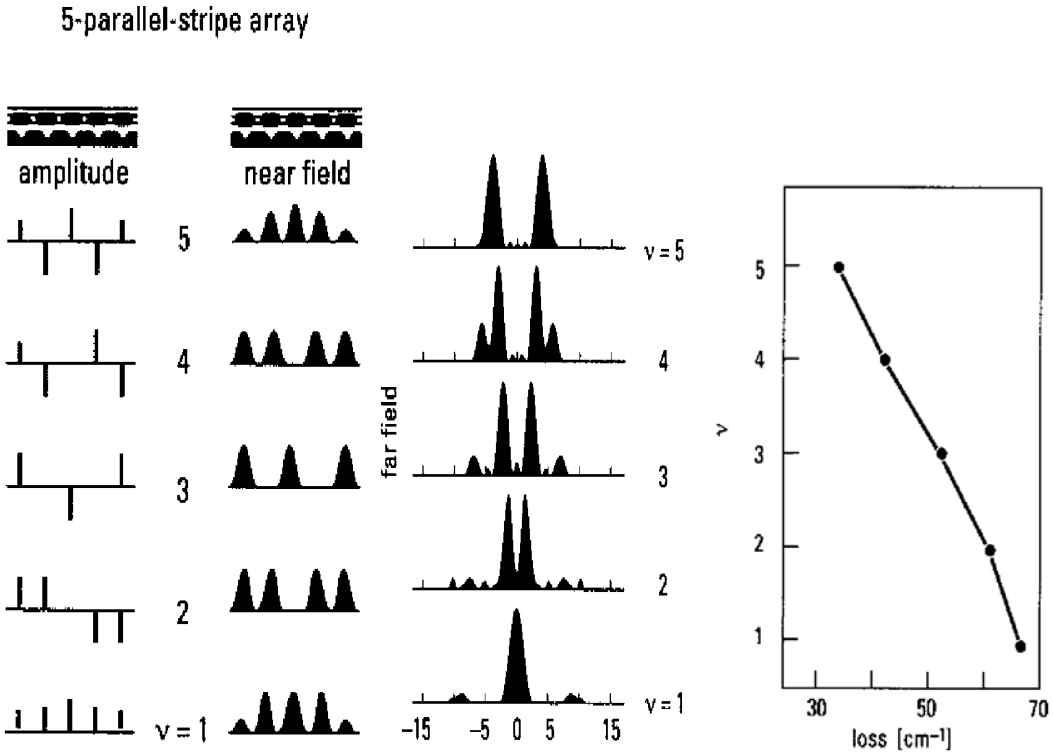

Fig. 2.1 Near fields and modal losses of supermodes in a parallel-stripe array of 5 identical stripes[39].

2.3 Two-dimensional laser array

Two-dimensional arrays typically have either a rectangular grid pattern or an annular ring pattern. Rectangular grid has two axes of translation symmetry, while annular ring has rotational symmetry, as shown in Fig. 2.2.

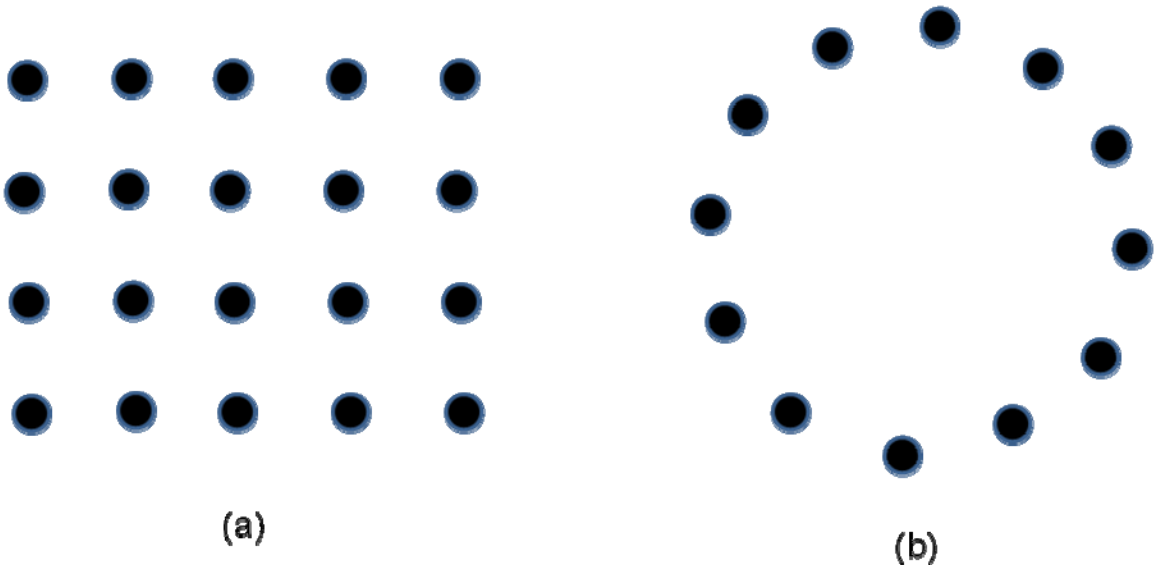

Fig.2.2 Two dimensional arrays in (a) rectangular grid pattern, and (b) annular ring pattern.

The same coupled-mode theory and the simple diffraction theory described in Section 2.2 can be applied to two-dimensional arrays to obtain their eigenmodes. General speaking, we can first define the electric field at near-field as a linear combination of all the emitting field, then apply the Fourier transform of the near-field to obtain the far-field.

As for a rectangular grid pattern, the phase difference among the elements is not easy to define analytically, except for the in-phase mode and out-of-phase mode, which are of most interest. By treating the grids as two orthogonal linear arrays, we can predict that the amplitude of the in-phase mode of a rectangular grid array is the highest at the center, lower at the edges, and the lowest at the corners. This unequal amplitude distribution inevitably results in higher energy extraction efficiencies at the center and lower efficiencies at the edges since the rate of stimulated emission is proportional to the laser power. In laser array with a large number of elements, the output power from the corners is nearly zero, leaving the pump energy mostly unutilized. Furthermore, the

unutilized pump energy leads to higher population inversion near edges, which tends to promote the higher order supermodes. Thus, from the efficiency and the mode control points of view, the rectangular grid pattern is not suitable for two-dimensional semiconductor laser arrays, which are coupled with nearest evanescent wave.

In contrast, all elements in the annular ring pattern array are expected to have the same output power and equal energy extraction efficiency because of the rotational symmetry. To apply the coupled mode theory to the annular array, we first determine the phase relation among the elements. With an array consisting *N* elements uniformly distributed on an annular ring. The N-fold periodic boundary condition requires the phase difference $\Delta\Phi$ between adjacent emitters is given as

$$\Delta\Phi_m = m2\pi / N \tag{2.4}$$

Where m is the mode index, *m=0,..., N-1*.

In the limit of weak coupling, we can model the electric field of the individual element as a Gaussian function, written as [16]

$$E(x,y,z) = \frac{1}{1 - i\frac{z}{z_0}} Exp\left[\frac{-(x^2 + y^2)}{\omega_0{}^2(1 - i\frac{z}{z_0})} + ikz\right] \tag{2.5}$$

Where ω_0 is the beam waist at the plane *z=0*, $z_0 = \pi\omega_0{}^2 / \lambda$ is the Rayleigh length, $k = 2\pi / \lambda$ is the wave number. The electric field of the supermode is a linear superposition of the electric field of individual elements with fixed phase relation. For m^{th} order supermode, the electric field at near-field is

$$E_m^{NF}(x,y,z) = \sum_{l=1}^{N} \frac{1}{1 - i\frac{z}{z_0}} Exp\{\frac{-[(x - x_l)^2 + (y - y_l)^2]}{\omega_0{}^2(1 - i\frac{z}{z_0})} + i(kz + l\Delta\Phi_m)\} \tag{2.6}$$

Using the same notation as Equations (2.4) and (2.5), l is the element number ranging, (x_l, y_l) is the center position of the l^{th} emitter. And the electric field at far-field is the Fourier transform of near-field, as

$$E_m^{FF}(u,v,z) = \mathcal{F}\{\ E_m^{NF}(x,y,z)\ \} \tag{2.7}$$

Where $\mathcal{F}$ is the Fourier transform operation evaluated at the spatial frequency $f \approx 1.22\theta/\lambda$, θ is the angular displacement from the center of the array, and λ is the wavelength of the field.

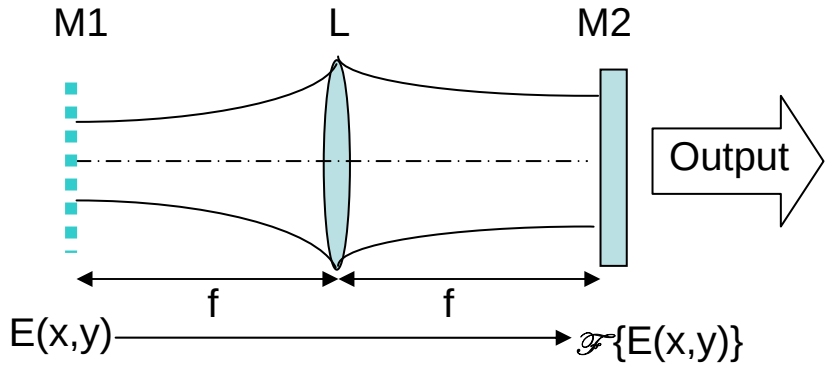

Fig. 1.2 Schematic of a self-imaging Fourier Transform resonator

In this thesis, laser arrays are coupled through a common Fourier transform resonator, as shown in Fig. 1.2. It can be shown that the electric fields at M1 andM2 are related to each other through a Fourier transform. So that we can write the electric field at M2 as

$$E_m^{FF}(u,v,z) = \mathcal{F}\{\ E_m^{NF}(x,y,z)\ \}$$

$$= \frac{1}{i\lambda f}\int_{-\infty}^{\infty} E_m^{NF}(x,y,z)\,Exp[-i\frac{2\pi}{\lambda f}(ux+vy)]dxdy$$

$$= \frac{\pi\omega_0^{\ 2}}{i\lambda f}Exp[i\frac{\pi^2\omega_0^{\ 2}}{\lambda^2 f^2}(i+\frac{z}{z_0})(u^2+v^2)+ikz]\sum_{l=1}^{N}Exp[-i\frac{2\pi}{\lambda f}(ux_l+vy_l)+il\Delta\Phi_m] \tag{3. 8}$$

As an example, we calculate the beam profiles of a 2X2 laser array, as shown in Fig.2.3.

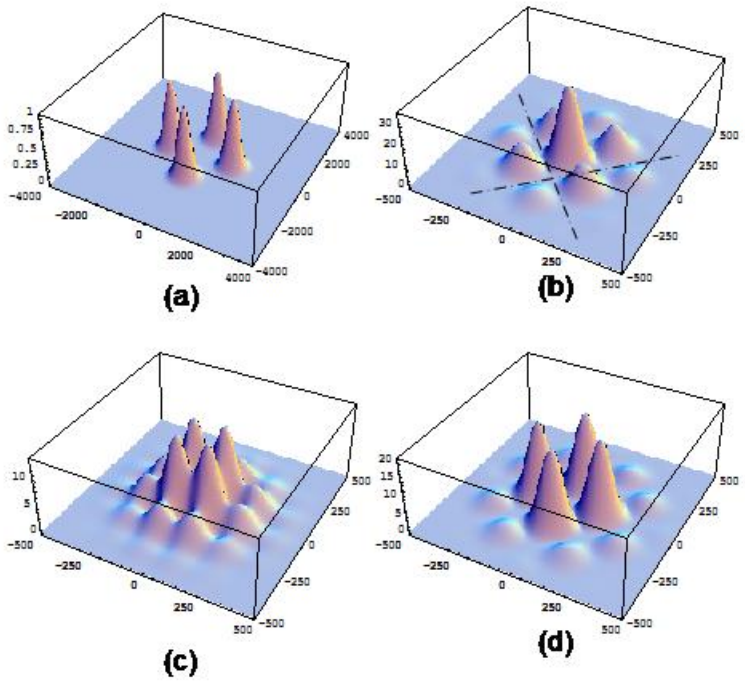

Fig.2.3 Beam profiles of 2x2 laser array: (a) emitters; (b) in-phase (m=0) mode; (c) m=1,3 mode; (d) out-of-phase (m=2) mode. The dashed lines mark the position for spatial filter for mode control.

2.4 Mode selection

According to the coupled-mode theory, an N-element laser array has N supermodes and the dominant supermodes are the ones with minimum loss. A mode selection mechanism is needed to produce desirable supermode. For an evanescent-wave coupled one-dimensional laser array, the highest order mode (out-of-phase) has minimal loss, while the lowest order mode (in-phase) has maximal loss. The laser array will operate in the out-of-phase mode unless a mechanism is introduced to promote the in-phase mode. In the Fourier transform resonator, mode selection can be done through an

intracavity spatial filter. The spatial filter is designed so that it causes minimal loss to the lowest order mode and higher losses to higher order modes. An example of spatial filter consisting of a pair of cross hairs positioned along the intensity minima of the in-phase mode is shown in fig.2.3 (b),

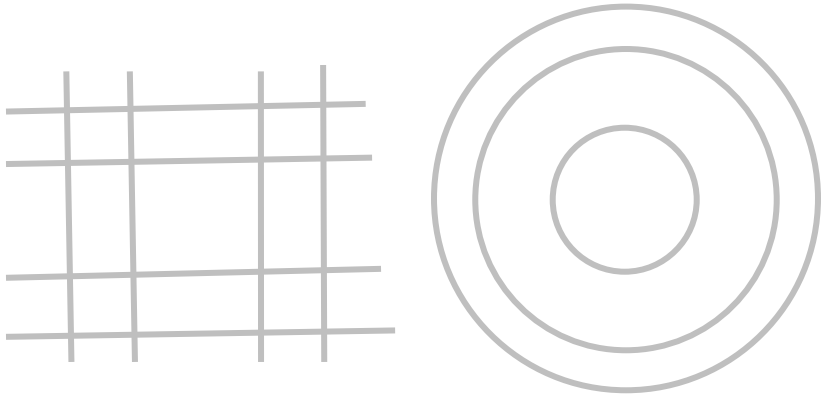

(a) (b)

Fig 2.4 Spatial filters for 2-D arrays, (a) in grid formation,(b) in annular formation.

2.5 Spatial filter and its losses

An appropriate spatial filter placed at the output coupler is used to select and stabilize the desired Gaussian-like beam profile. For a two-dimensional arrays in the rectangular formation, the filter consists a set of straight opaque lines along the intensity minimum of the in-phase modes to cause higher losses of higher-order modes while causing negligible loss to the in-phase mode, as shown in Fig. 2.4 (a); for an array in annular formation, a filter consisting of a set of concentric opaque rings does the same job, as shown in Fig. 2.4(b).

To find the losses due to the spatial filter, we define the overlapping efficiency of the field at near field as

$$\eta_m = \frac{\left|\int_{-\infty}^{\infty} E_m^{NF*}(x,y,0)\cdot F\{E_m^{FF}(u,v,0)\}dxdy\right|}{\int_{-\infty}^{\infty}\left|E_m^{NF}(x,y,0)\right|^2 dxdy} \tag{2.9}$$

Without the spatial filter, η_m=100% for any m mode. This means the Fourier transform resonator supports all the N supermodes, each having the same resonator loss without the spatial filter. In the presence of spatial filter on the output mirror, the field $E_m^{FF}(u,v,0)$ is zero along the apaque lines. And the overlapping efficiency is

$$\eta_m = 1-\sum_i \frac{\left|\int_{-\infty}^{\infty} E_m^{NF*}(x,y,0)\cdot F\{E_m^{FF}(r_i,\Delta\omega_i)\}dxdy\right|}{\int_{-\infty}^{\infty}\left|E_m^{NF}(x,y,0)\right|^2 dxdy} \tag{2.10}$$

Where $E_m^{FF}(r_i,\Delta\omega_i)$ is the field of obstructed area at spatial filter. The second term is referred to the losses due to spatial filter.

$$\text{L}=\sum_i \frac{\left|\int_{-\infty}^{\infty} E_m^{NF*}(x,y,0)\cdot F\{E_m^{FF}(r_i,\Delta\omega_i)\}dxdy\right|}{\int_{-\infty}^{\infty}\left|E_m^{NF}(x,y,0)\right|^2 dxdy} \tag{2.11}$$

Alternatively, L can be simply calculated from transmission of the beam.

$$\text{L}=\frac{\sum_i \int_0^{2\pi}\int_{r_i-\Delta\omega_i/2}^{r_i+\Delta\omega_i/2}\left|E_m^{FF}(r_i,\Delta\omega_i)\right|^2 rdrd\theta}{\int_{-\infty}^{\infty}\left|E_m^{FF}(u,v,0)\right|^2 dudv} \tag{2.12}$$

Chapter 3 Neodymium-doped solid-state lasers

Neodymium-doped yttrium aluminum garnet (Nd:YAG) and neodymium-doped yttrium vanadate (Nd:YVO_4) crystals have been used as the gain media for the work reported in this thesis. This chapter provides a summary of their physical and optical properties.

3.1 Introduction

Neodymium (Nd) is a member of the rare-earth group of elements within the periodic table, all of which have the general electronic structure $4f^N 4s^2 5p^6 5d^0 6s^2$, where N ranges from 1 to 14. In particular, Nd has the structure $(Xe)4f^4 5p^6 6s^2$. When incorporated into a host material, the outer two 6*s* electrons of Nd atom and one of the 4*f* electrons are used for ionic binding, so Nd becomes triply ionized.

Nd^{3+} was the first of the trivalent rare earth ions to be used in a laser, and it remains by far the most important element in this group. Stimulated emission has been obtained with this ion incorporated in at least 100 different host materials. The principal host materials are YAG (yttrium aluminum garnet), YLF (yttrium lithium fluoride), YVO_4 (yttrium orthovanadate), and glass. A particular host material is chosen in order to obtain a desired combination of optical, mechanical, and thermal properties. Nd:YAG lasers and variants are optically pumped using flashlamps or laser diodes. In these hosts stimulated emission is obtained at a number of frequencies within three different groups of transitions centered are 0.9 μm, 1.06 μm and 1.32 μm. Radiation at these wavelengths

results from ${}^4F_{3/2} \rightarrow {}^4I_{9/2}$, ${}^4I_{11/2}$, and ${}^4I_{13/2}$ transitions, respectively, as shown in the energy level diagram of Nd^{3+} (Fig 3.1) [40].

Based on its energy levels, laser transitions from Nd^{3+} are typically a four-level system. Exception for the ground-state transition around 0.9–0.95 μm is a three-level system. A four-level system laser has a lower threshold pump power, because the lower laser level is well above the ground state and is quickly depopulated by multiphonon transitions. The gain usually rises linearly with the absorbed pump power.

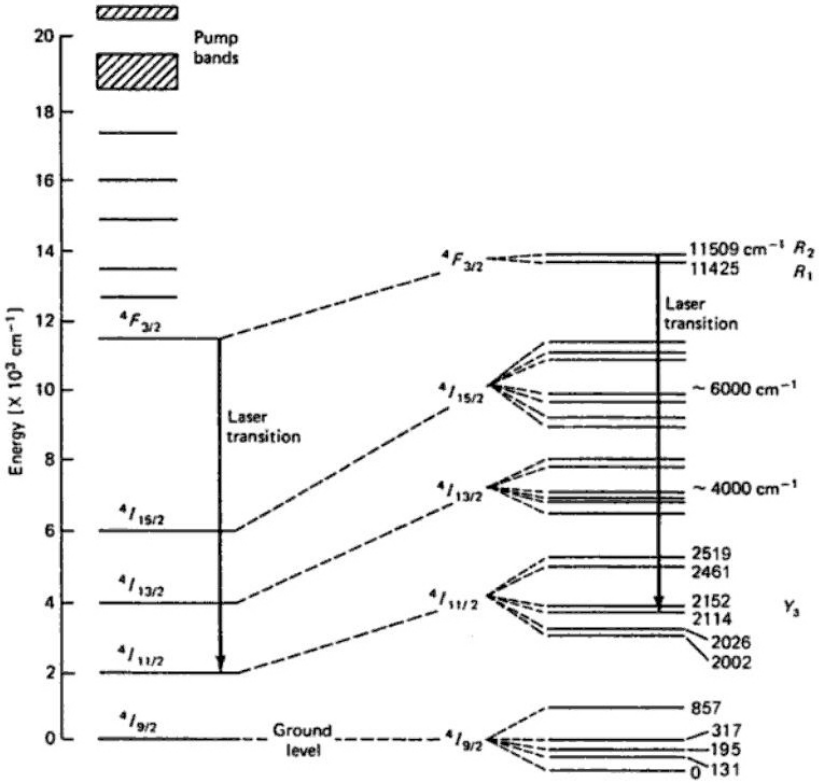

Fig. 3.1 Energy level diagram for Nd:YAG [40].

3.2 Nd: YAG Lasers

The Nd:YAG laser is by far the most commonly used solid-state laser. Nd: YAG possesses a combination of properties uniquely favorable for laser operation. Pure YAG is a colorless, optically isotropic crystal possessing a cubic structure characteristic of garnets. In Nd:YAG about 1% trivalent yttrium is substituted by trivalent neodymium because they are of similar sizes . The radii of the two rare earth ions differ by about 3%. No charge compensation is required in Nd:YAG. The Nd:YAG crystal is hard, of good optical quality, and has a high thermal conductivity. Furthermore, the cubic structure of YAG favors a narrow fluorescent linewidth, which results in high gain and low threshold for laser operation. Some of the important physical properties of Nd:YAG are listed in Table 3.1 together with its thermal and optical properties [40].

Table 3.1 Physical, optical and thermal properties of Nd:YAG

Property	Value
chemical formula	$Nd^{3+}:Y_3Al_5O_{12}$
crystal structure	Cubic
mass density	4.56 g/cm^3
Moh hardness	8 to 8.5
Young's modulus	280 GPa
tensile strength	200 MPa
melting point	1970 °C
thermal conductivity	13 to 14 W / (m K)
thermal expansion coefficient	7 to $8 \cdot 10^{-6}$/K
thermal shock resistance parameter	790 W/m
birefringence	none (only thermally induced)
refractive index at 1064 nm	1.82
temperature dependence of refractive index	7 to $10 \cdot 10^{-6}$/K
Nd density for 1% atm. doping	$1.36 \cdot 10^{20}$ cm^{-3}
fluorescence lifetime	230 μs
absorption cross section at 808 nm	$7.7 \cdot 10^{-20}$ cm^2
emission cross section at 1064 nm	$28 \cdot 10^{-20}$ cm^2
gain bandwidth	0.6 nm

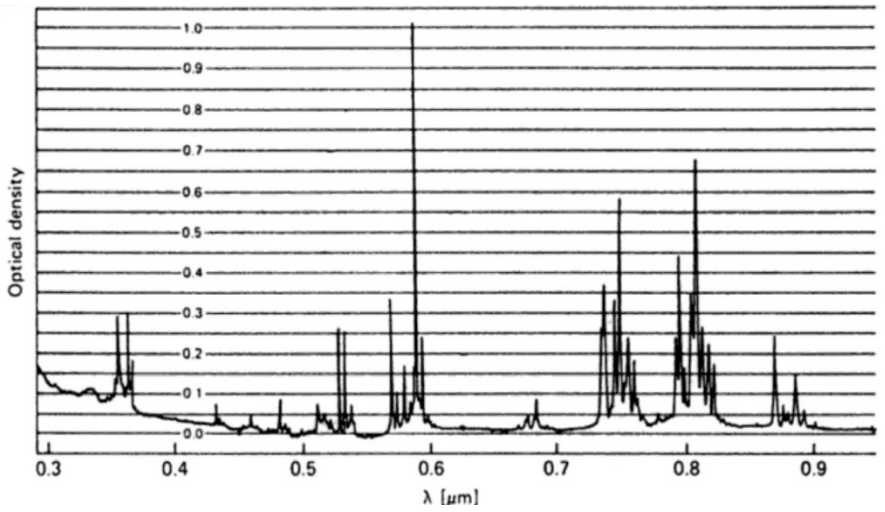

Fig. 3.2 Absorption spectrum of Nd:YAG at 300 K[40].

The absorption spectrum of Nd:YAG is given in Fig 3.2. Nd:YAG absorbs mostly in the bands between 730-760 nm and 790-820 nm. The strongest peak centered around the wavelength of 808 nm is important for diode pumping. Under normal operation conditions the Nd:YAG laser oscillates at room temperature on the strongest ${}^4F_{3/2} \rightarrow {}^4I_{11/2}$ transition at 1.0641 μm. The fluorescence spectrum is shown in Fig. 3.3. Due to these favorable properties, Nd:YAG is widely used in high-power lasers and Q-switched lasers emitting at 1064 nm.

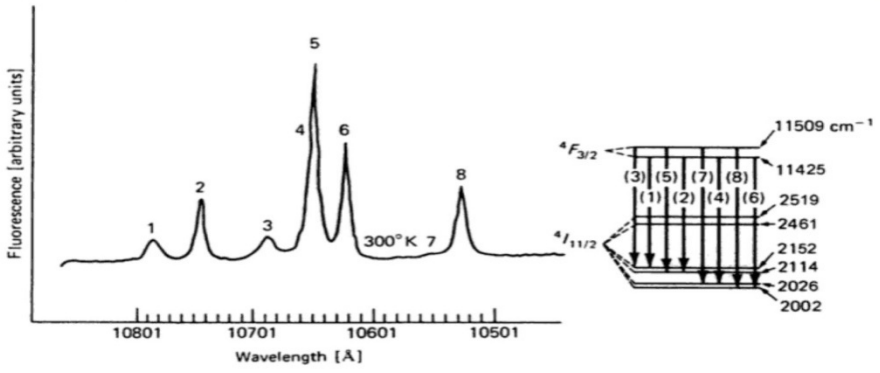

Fig. 3.3 Fluorescence spectrum of Nd^{3+} in YAG at 300 K in the region of 1.06 μm [40].

3.3 Q-switched Nd lasers

Pulsed Nd:YAG lasers are typically operated in the Q-switching mode via either active or passive Q switching. For active Q switching, an active control element, typically either an acousto-optic or electro-optic modulator, is inserted in the laser cavity. This introduces higher loss in the resonator while the gain medium is being pumped and abruptly reduces the losses to allow the laser action to start when the level of population reaches the maximum level. For passive Q switching, the Q-switch is a saturable absorber, a material whose transmission increases when the intensity of light exceeds some threshold, as shown in Fig. 3.4 [40]. The material may be an ion-doped crystal like Cr:YAG, which is used for Q-switching of Nd:YAG lasers, a bleachable dye, or a passive semiconductor device. Initially, the loss of the absorber is high, but still low enough to permit lasing action to initiate once the inversion level reaches the threshold. As the laser power increases, it saturates the absorber, and thereby, rapidly reduces the resonator loss, so that the power further increases. This positive feedback process brings the absorber into a state with low losses to allow efficient extraction of the stored energy by the laser pulse.

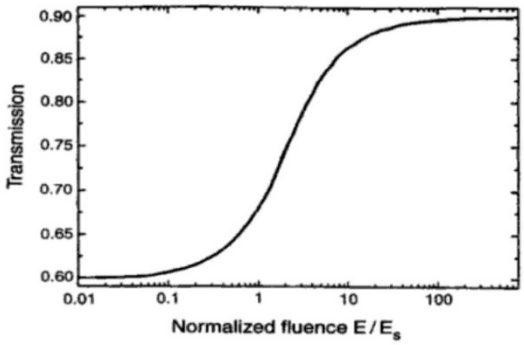

Fig. 3.4 Nonlinear transmission of a saturable absorber [40]

To date, the most commonly used passive Q-switch is Cr^{4+}:YAG, in which the Cr^{4+} ions provide the saturable loss in the wavelength range from 900 nm to 1200 nm. The absorption recovering time ranges 3-8 μs depending on the concentration of Cr^{4+}.

When YAG host crystals are co-doped with Nd^{3+} and Cr^{4+}, the functions of the gain medium and the saturable absorber are combined into one. Compact, efficient, highly polarized and highly stable passively Q-switched lasers have been developed based on Cr,Nd:YAG [41-43]. Because Nd^{3+} , Cr^{3+} andCr^{4+} are present in the YAG, the room-temperature absorption spectrum of Cr,Nd:YAG, as shown in Fig. 3.5, consists of the absorption features of all three ions. The sharp lines at 0.53, 0.59, 0.75, 0.81, and 0.88 μm are attributed to Nd^{3+} ions. The broad absorption bands centered at 0.43 and 0.59 μm are attributed to the $^4A_2 \rightarrow {}^4T_1$, and $^4A_2 \rightarrow {}^4T_2$ transitions of Cr^{3+}. The band from 900 to 1200 nm is believed to be caused by Cr^{4+} ions [41].

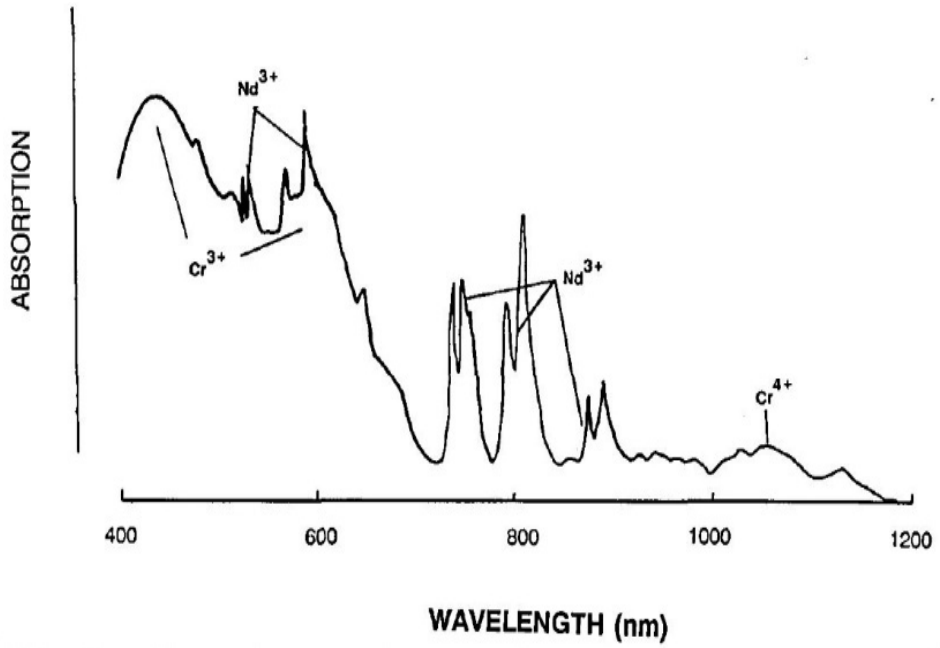

Fig. 3.5 Room-temperature absorption spectrum of Cr,Nd:YAG[41].

3.4 Nd: YVO4 lasers

Nd:YVO_4 is one of the most efficient solid-state laser crystals. Its physical, thermal and optical properties are summarized in Table 3.2. Compared with Nd:YAG , Nd:YVO_4 has several spectroscopic properties which are particularly relevant to laser diode pumping. The two outstanding features are the large stimulated emission cross-section (five times higher than that of Nd:YAG), and a strong broadband absorption at 809 nm which allows diode pumping with a relaxed requirement for the wavelength of the diode laser.

Table 3.2: Physical, optical and thermal properties of Nd:YVO_4 [40]

Property	Value
chemical formula	Nd^{3+}:YVO_4
crystal structure	tetragonal
mass density	4.22 g/cm^3
Moh hardness	5–6
Young's modulus	133 GPa
tensile strength	53 MPa
melting point	1810 °C
thermal conductivity	□ 5 W / (m K)
thermal expansion coefficient	11×10^{-6} K^{-1} (*c* direction), 4.4×10^{-6} K^{-1} (*a* direction)
transparency range	0.3–2.5 μm
birefringence	positive uniaxial
refractive index at 1064 nm	2.17 for *c* polarization (extraordinary), 1.96 ordinary index
temperature dependence of refractive index	3×10^{-6} K^{-1} in *c* direction, 8.5×10^{-6} K^{-1} in the *a* direction
Nd density for 1% at. doping	1.24×10^{20} cm^{-3}
fluorescence lifetime	90 μs
absorption cross section at 808 nm	60×10^{-20} cm^2 (*c* polarization)
emission cross section at 1064 nm	114×10^{-20} cm^2 (*c* polarization)
gain bandwidth	1 nm

Nd:YVO_4 is naturally birefringent and its laser output is linearly polarized along the extradinary π-direction. Pump absorption in this uniaxial crystal is also polarization dependent. The strongest absorption occurs for pump light polarized in the same direction

as laser radiation. The absorption coefficient is about four times higher compared to Nd:YAG in the π-direction.

Nd:YVO4 lasers possess the advantages of lower dependency on pump wavelength and temperature control of a diode laser, a wide absorption band, higher slope efficiency, lower lasing threshold, linearly polarized emission and single-mode output. For Q-switched lasers, Nd:YVO_4 does not allow for pulse energies as high as Nd:YAG due to the shorter excited state lifetime. It is better suited for high pulse repetition rates, where it still allows the generation of fairly short Q-switched pulses [40].

Chapter 4 Ytterbium fiber lasers

4.1 Double-clad fibers

Fiber lasers are advancing rapidly in the last ten years. Fiber lasers have the advantages of high efficiency, simpler design, and excellent beam quality. The fiber geometry increases the surface-to-volume ratio and makes it easier to dissipate the heat. In addition, fiber lasers are normally easier to maintain compared with bulk glass lasers. They can operate over a long time span with high reliability.

The typical core diameter of a single-mode fiber is on the order of several microns. The small size of the core makes it difficult to deliver high-power pump beam into the core directly because most pump laser beams are spatially incoherent and cannot be focused to the core. Double-clad fibers are designed to ensure the single-mode operation of the laser while allowing the pump beam to be efficiency collected in the cladding and subsequently absorbed by the lasing ions in the core as the beam propagates along the fiber and makes multiple passes through the core. The schematic drawing of a double-clad fiber is shown in Fig.4.1. These fibers typically consist of a rare-earth doped core, an un-doped inner cladding, and an outer cladding. The double clad fiber is designed such that the core can only support a single spatial mode of the lowest order. The inner cladding has high numerical aperture and a large diameter typically in the range of hundreds of microns to allow the incoherent pump beam be collected with high efficiency. The inner cladding shape is often non-circular to suppress the helical the modes, whose paths do not pass through the core, so that the power distribution of the pump better overlaps with the core. The core can also be offset from the center to improve the

efficiency [44]. The pump conversion efficiency in double-clad fibers can be as high as 83% [45].

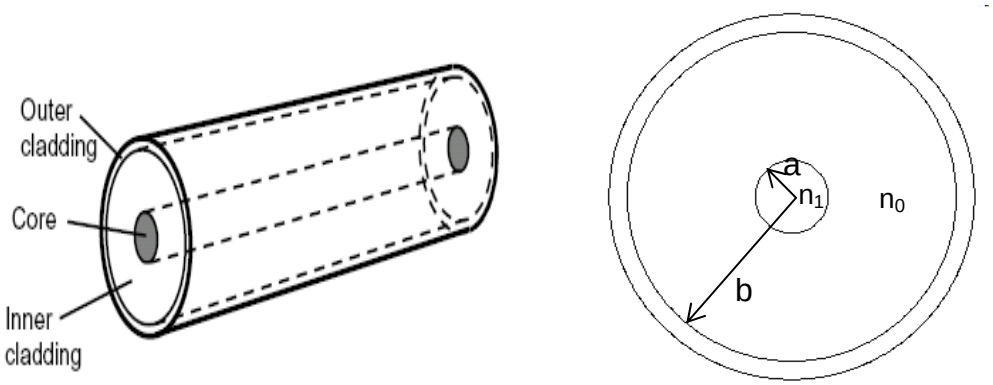

(a) (b)

Fig. 4.1 Schematic drawing of a double-clad fiber. (a) Side view (b) end view. The index of refraction is n_1 in the core, and n_0 in the inner cladding. The outer cladding is made of low-index polymers.

The number of propagating modes allowed for a waveguide shown in Fig.4.1 (b) is given [46] as

$$N \approx \frac{V^2}{2} = \frac{1}{2}\left(ka\sqrt{2\frac{\Delta n}{n_1}} \right)^2 \tag{4.1}$$

where V is the V-number of the fiber, k is the wave number and Δn is the difference in refraction indices between the core and the inner cladding . The ytterbium double clad fiber used in this thesis has a core diameter of 5 micron and Δn =0.0077, n_1=1.46. The number of modes is N~1.

High optical power in the core can lead to optical damage in the fiber, especially at the end surfaces. The optical damage threshold in silica fibers is about 10 W/μm^2 [47]. A fiber is required to have a core area of 1000 μm^2 for 10 kW output power. Larger core size results in multi-mode operation in the fiber cavity. By coiling the fiber,

significant loss can be induced to the higher-order mode to allow the fundamental mode to operate in multimode fibers. Fundamental-mode operation in a 2000 μm^2 fiber core area has been achieved with the coiling technique [48].

Thermal management is important for high-power fiber lasers. In fiber lasers less than 15% of the pump energy is converted into heat due to high conversion efficiencies [49]. The fiber geometry allows the heat to be distributed over a long length. Air cooling is usually sufficient.

Nonlinear effects play an important role in high power fiber lasers and can impose a limitation on the highest power achievable in fiber lasers. Nonlinear effects are induced by the large power density in the small area of fiber core. Among the nonlinear effects, Brillouin backscattering can be the limitation of the output power for narrow-band signals; and Raman scattering can generate a large frequency shift. The threshold power density is on the order of MW/cm^2 for the onset of Brillouin scattering and GW/cm^2 for Raman scattering. Although the nonlinear effects may be suppressed by enlarging the core diameter which reduces the power density inside the fiber and by shortening the fibers length to reduce the gain length for nonlinear conversion, the large core can result in multimode operation and the shorter fiber length reduces the total volume for energy storage. Shorter fiber length may also suffer from thermal effects resulting in lower efficiency.

Eventually, the output of a single fiber laser will reach a limit and further increase of laser output can be achieved only through coherent combination of the output of a number of fiber lasers.

4.2 Ytterbium doped silica fiber

Both Nd and Yb are suitable doping elements for high-power fiber lasers. Both can emit light around 1060 nm. The peak of the absorption spectrum of neodymium ions is at 808 nm, while Yb is at 975 nm. Nd works as a four-level system near 1060 nm. It has a relatively low laser threshold, while Yb works as a three-level system at 1060nm. In a three-level system, the lower level of laser transition is so close to the ground state that an appreciable population in that level occurs in thermal equilibrium at the operating temperature. As a consequence, the unpumped gain medium causes some reabsorption loss at the laser wavelength and transparency is reached at a higher level than in the four-level system. For ytterbium, the disadvantage of the three-level system is more than offset by the higher concentration of ytterbium ions and the smaller quantum defects. This results in the photon energy of the emitted photons being closer to that of the pump photons. These advantages make ytterbium more attractive than neodymium as a doping element in fiber laser systems. Yb-doped double cladding fibers are used in the experiments of this thesis.

Compared to other rare-earth ions, the Yb^{3+} energy level structure is a simple one, as shown in Fig. 4.2(a), consisting of only two manifolds: the ground energy manifold $^2F_{7/2}$ and the excited energy manifold $^2F_{5/2}$. The Stark effect makes the excited manifold split into three sublevels and the ground manifold split into four sublevels. From the energy level diagram, it can be seen that there is no excited-state absorption at the pump or laser wavelength. In addition, because of the large energy gap between the ground manifold and the excited manifold, there is small possibility of multi-phonon emission

from the excited manifolds. Thus little concentration quenching occurs for ytterbium in silica.

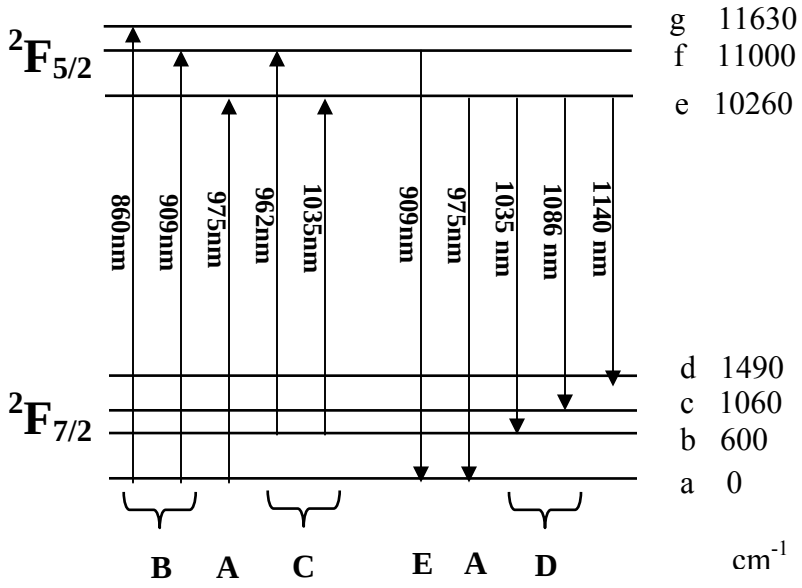

(a)

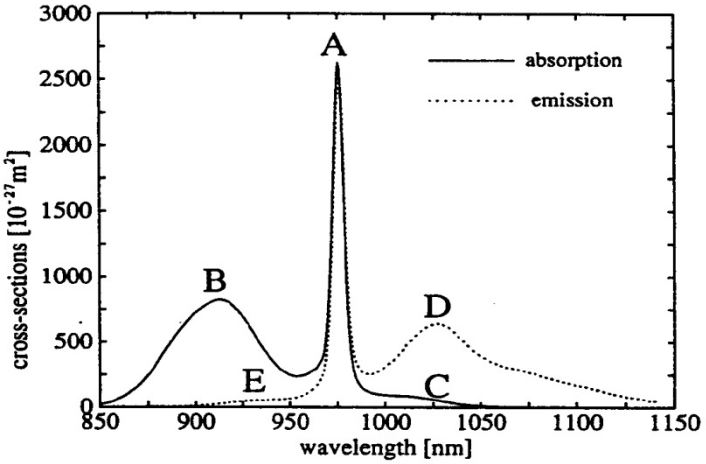

(b)

Fig. 4.2. (a) The Yb^{3+} energy level structure, consisting of two manifolds, the ground manifold $^2F_{7/2}$ (with four Stark levels, labeled (a)-(d)), and a well separated excited manifold $^2F_{5/2}$(with three Stark levels labeled (e)-(g)).Approximate energies in wave numbers above ground energy are indicated. (b) Absorption and emission cross sections for a germanosilicate host [50].

The energy level diagrams can be matched with the absorption and emission lines. As shown in Fig. 4.2(b), peak A in the absorption and emission spectra is generated by

the energy transfer between the lowest stark levels in each manifold. Peak B corresponds to the f to g absorption, and peak C corresponds to b-to-g transition. Peak C of the absorption spectrum can produce re-absorption in the Yb^{3+} doped medium, which increases the thresholds of fiber laser systems operating around 1000 nm. Peak D in the emission spectrum corresponds to transitions from e to b, c and d. In these transitions, the energy sublevels c and d are almost empty so it can be treated as a four level system. Peak E corresponds to the transition from the sublevel f, which generates very weak emissions in most situations. Pumping at the strong absorption peak (A) at 975 nm enables efficient pump absorption in short fiber length. To minimize the absorption length, the experiments in this thesis have used diode pumping at wavelengths close to the 975 nm absorption peak [50].

4.3 Stimulated Raman and Brillouin scatterings in optical fiber

Nonlinear effects are significant in optical fibers due to the high optical intensity in the small core and the long propagation lengths. The onset of nonlinear effects sets the upper limit to the power density of a fiber laser. In some cases, these effects can be beneficial when properly utilized. In this thesis, short pulses are generated by using Brillouin backscattering as a distributed passive *Q*-switching mechanism

Raman and Brillouin scattering are inelastic processes in which part of the power is lost from an optical wave and absorbed by the transmission medium while the remaining energy is re-emitted as a wave of lower frequency. The processes can be thought of as the conversion of an incident photon into a scattered photon of lower energy plus a phonon of vibrational energy. The total energy and momentum before and

after scattering must be conserved, i.e. the incident photon energy is shared between the phonon and the scattered photon. Since the frequency of an optical wave is proportional to its energy, the photon produced by the scattering event has a lower frequency than the incident photon. This frequency downshifted wave is commonly referred to as the *Stokes wave*. Stimulated Brillouin scattering (SBS) occurs at low threshold optical power density of MW/cm^2 while Stimulated Raman scattering (SRS) occurs at a typical threshold power density of GW/cm^2. It is the lower threshold that makes SBS a dominant nonlinear process in optical fibers.

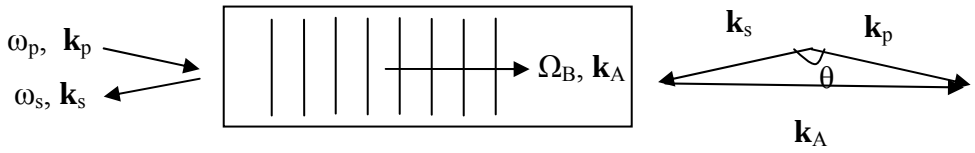

Fig. 4.4 Stimulated Brillouin scattering [51]

The process of SBS can be described classically as a nonlinear interaction between the pump and Stokes fields through an acoustic wave, shown in Fig. 4.4. The pump field generates an acoustic wave through the process of electrostriction [51]. The acoustic wave in turn modulates the refractive index of the medium. This pump-induced index grating scatters the pump light through Bragg diffraction. The scattered light is downshifted in frequency because of the Doppler shift associated with a grating moving at the acoustic velocity v_A. The same scattering process can be viewed quantum-mechanically as if the annihilation of a pump photon creates a Stokes photon and an acoustic phonon simultaneously. As both energy and momentum must be conserved during each scattering event, the frequencies and the wave vectors of the three waves are related by

$$\Omega_B = \omega_p - \omega_s, \quad \mathbf{k}_A = \mathbf{k}_p - \mathbf{k}_s \tag{4.2}$$

Where ω_p and ω_s are the frequencies, and $\mathbf{k}_p$ and $\mathbf{k}_s$ are the wave vectors, of the pump and Stokes wave, respectively.

The frequency Ω_B and the wave vector $\mathbf{k}_A$ of the acoustic wave satisfy the standard dispersion relation

$$\Omega_B = v_A |K_A| \approx 2 v_A |K_p| \sin(\theta/2) \tag{4.3}$$

Where θ is the angle between the pump and Stokes fields, and we used $|K_p| \approx |K_s|$ in Equation (4.2). Equation (4.3) shows that the frequency shift of the Stokes wave depends on the scattering angle. In particular, Ω_B is maximum in the backward direction (θ=π) and vanishes in the forward direction (θ=0). In a single-mode optical fiber, the only relevant directions are the forward and backward directions. For this reason, SBS occurs only in backward direction [52].

Similarly, the process of SRS can be described classically as a nonlinear interaction between the pump and Stokes fields through a low frequency photon. The same analysis can be applied to an SRS process, where the frequency shift Ω_R is given as

$$\Omega_R = v_L |K_L| \approx 2 v_L |K_p| \cos(\theta/2) \tag{4.4}$$

where Ω_R,v_L, and $\mathbf{k}_L$ are the frequency, velocity and wave vector of the scattered photon, respectively, θ is the angle between the pump and Stokes fields, $\mathbf{k}_p$ is the wave vector of the pump. We used $|K_p| \approx |K_s|$ in Equation (4.2). Ω_R is maximum in the forward direction (θ=0) and vanishes in the backward direction (θ=π). Thus SRS occurs mostly in forward direction.

Since SBS associates with an acoustic phonon, while SRS associates with an optical photon, the difference in frequency between the pump and Stokes waves is

therefore much lower in SBS than in SRS. Typical values of the pump-Stokes frequency difference are 10-GHz (~0.1-nm at 1550-nm) for SBS and 13-THz (~110-nm at 1550-nm) for SRS. SBS limits the maximum optical power that can be launched into a fiber since any power above the SBS threshold is reflected backward. SRS that is shifted from the pump wave by 10 to 100-nm while propagating forwards along the fiber with the pump wave will decrease the pump and signal power.

Chapter 5 Phase locking of Nd:YVO_4 laser array

This chapter describes the phase locking of a two-dimensional continuous-wave Nd:YVO_4 laser arrays by using the Fourier transform resonator.

5.1 Experimental

The schematic of the experimental setup is illustrated in Fig. 5.1. A Nd:YVO_4 crystal is end-pumped by four continuous-wave pump beams from four optical fibers, each delivering 1 W at 808 nm. The resonator terminates on one side in a flat-output mirror (M2) with 6% transmission at 1064 nm and on the other side on the surface of the Nd:YVO_4 plate (M1) coated for high reflectivity at 1064 nm and 96% transmission at 808 nm. Mirrors M1 and M2 were located on the focal planes on each side of the converging lens. For the convenience of being able to construct the spatial filter using easily available thin metal wires, the focal length is chosen to be 40 cm. A much shorter focal length may be used with finer grid patterns made by, for example, photolithography. The 1-mm-thick vanadate crystal, containing 2 atm% Nd doping is surface-cooled through contact bonding with a sapphire crystal. The uncoated bonding interface between Nd:YVO_4 and sapphire has a 0.4% residual reflectance. The optical fibers for delivering the pump beams have a core diameter of 200 μm and numerical aperture of 0.39. The fibers are symmetrically positioned at the corners of a square with various separations ranging from 0.5 to 1 mm between adjacent elements. Two charge-coupled device (CCD) cameras are used to monitor the beam profiles at near field M1 and at far field M2.

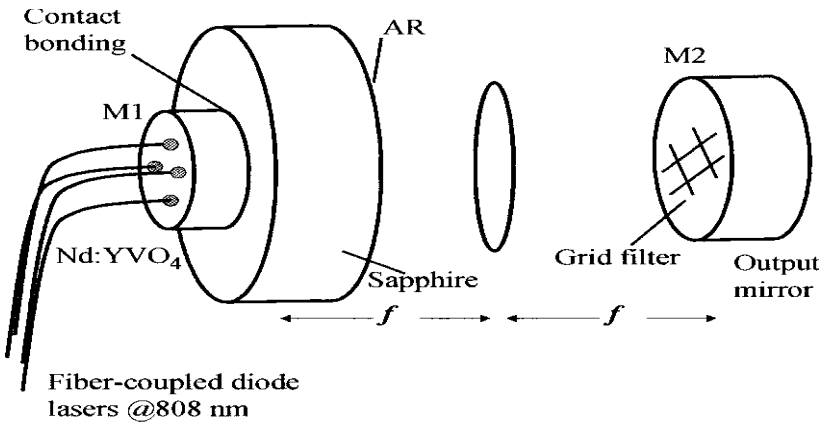

Fig. 5.1 Schematic of phase-locking a 2x2 laser array in a Fourier transform resonator

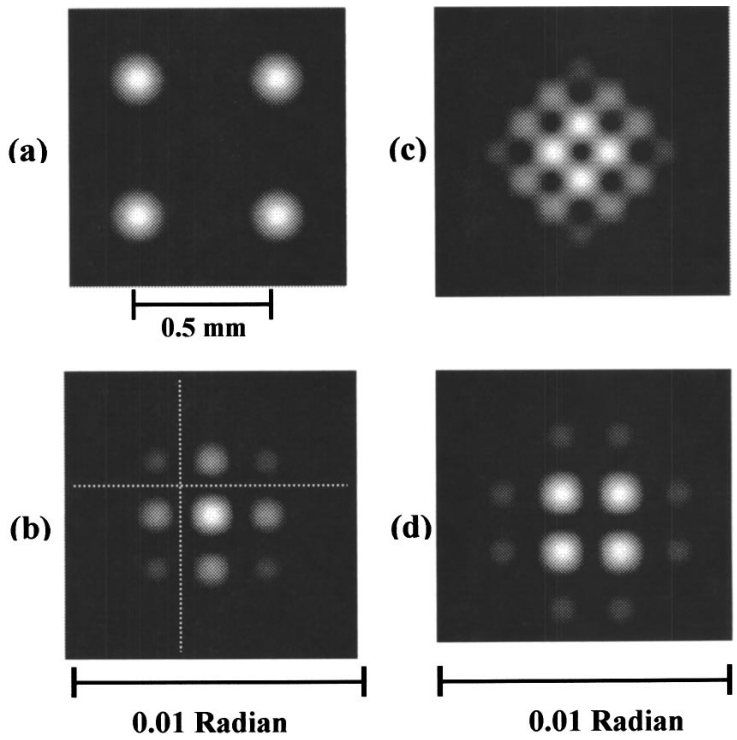

Fig. 5.2 Beam profiles (a) at the emitters, and in the far field for four coherent Gaussian beams with various phase difference between adjacent elements.(b) $\Delta\Phi=0$, (c) $\Delta\Phi=\pi/2$, $3\pi/2$, and (d) $\Delta\Phi=\pi$ The dotted lines mark the position for spatial filter for mode control.

5.2 Results and discussion

There are four supermodes that can oscillate within the resonator. Numerical beam profiles at near field and far field are presented as shown in Fig. 5.2. Phase locking

operation in fundamental transverse mode with high stability and high efficiency was achieved in experiment.

For an inter-element separation of 500 μm, the evanescent-wave coupling between adjacent elements results in the operation of the out-of-phase mode at the threshold when a uniform output mirror is used. As the pump power increases, the competition among the transverse modes results in beam instability. By placing a pair of tungsten cross hairs of 20-μm diameter along the intensity minima of the predicted modal patterns at the output mirror, the laser operates stably in the in-phase or out-of-phase modes, shown in Fig. 5.3, Once the spatial filter is in place, stable operation in either mode has been obtained at all pump powers up to twofold excess of the threshold, without mode competition or beam movement. The full width at half maxima of the central lobe of the in-phase mode is 1.1 mrad and remains unchanged with pump power.

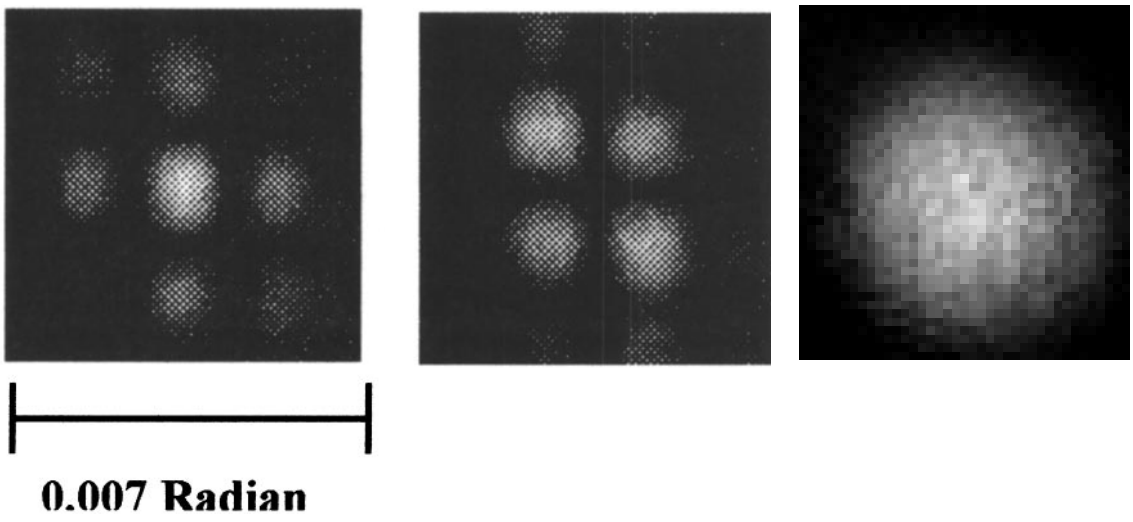

Fig. 5.3 Beam profiles of (a) in-phase mode, (b) out-of-phase mode at 500 mW output power, and (c) a single element.

The pump power conversion efficiencies of the aser array operating in all modes without the spatial filter, and in the in-phase mode are shown in Fig.5.4. The slope efficiency is 53% for all modes and 49% for the in-phase mode. The presence of the spatial filter results in a slight increase in threshold however the slope efficiency of the in-phase mode is still higher than the slope efficiency of 48% when only one element is operating.

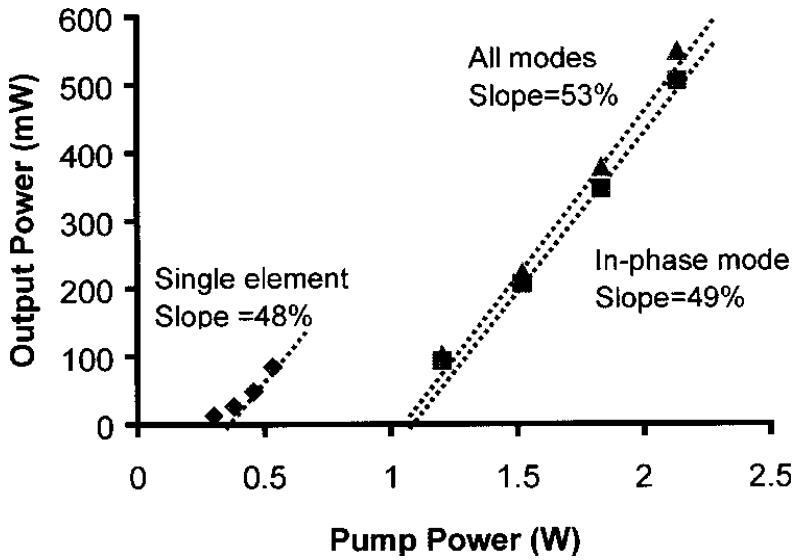

Fig. 5.4 Output power vs. input power characteristics of the four-element laser array. The characteristics of a single element are shown for comparison.

The phase locking is quite insensitive to power variations among the pump beams. For example, with the spatial filter in place, the beam profile of the in-phase mode is nearly unaffected when one of the pump beams is completely turned off. The combined pump power at threshold also remains unchanged because the other three elements deliver 33% higher pump power to compensate for the missing fourth element. The missing element appears to be ‘‘repaired’’ by the image of the diagonal element after one round trip.

Two considerations related to the properties of Nd:YVO_4 crystal have been taken into account to achieve phase locking. First, Nd:YVO_4 has a narrow gain bandwidth of 0.96 nm (257 GHz). Thus there is strict requirement in parallelism of the Nd:YVO_4 crystal to ensure the frequencies of all elements lie within the gain bandwidth. Second, the Nd:YVO_4 crystal has low thermal conductivity. To avoid thermal lensing, the Nd:YVO_4 crystal is surface cooled by bonding a sapphire disc heat sink to the crystal to allow better heat dissipation. Furthermore, this phase locking scheme is a hybrid of evanescent wave coupling and common resonator coupling. In order to get a good fill factor and minimize evanescent wave coupling, elements need to be optimally arranged.

5.3 Conclusion

We demonstrated phase locking in a two-dimensional solid-state laser array through common Fourier transform resonator. Beam control in the far field of the emitters involves simpler beam profiles compared to the Talbot resonator, which utilizes diffraction. We have demonstrated phase locking in a two-dimensional solid-state laser array through a common Fourier-transform resonator. Modal selection is accomplished by controlling the beam profile and using a spatial filter on the output coupler. Beam control in the far field of the emitters involves simpler beam profiles compared to the near field approaches, such as the Talbot resonator. Phase locking through a Fourier-transform resonator has the advantage of high feedback efficiency, relaxation of requirement from purely periodic to inversion symmetric structure of emitters, less sensitivity to power variations among the elements, and the ability to repair a missing element. This approach can be applied to laser arrays with a large number of elements.

Chapter 6 Phase locking of short-pulse Q-switched lasers

6.1 Introduction

To date, most of the studies have concentrated on phase locking of the continuous-wave (CW) or long pulsed lasers with multiple gain elements. Few studies have been done on the behavior of phase-locked pulsed lasers. For CW lasers, the phase-locked state is characterized by a time-independent interference fringe pattern in the far field where the laser beams from the individual elements overlap. In our experimental study of the two-dimensional laser array described in Chapter 5, the laser elements are formed on a single crystal with a high-degree of parallelism. This results in a common operating frequency can be found within the gain bandwidth, even though the optical path lengths of the individual elements might be slightly different. Little consideration in the time domain is needed. In short-pulse lasers, however, the conditions for phase locking differ from those of the continuous-wave lasers in two ways. Firstly, two or more pulsed lasers operating at slightly different frequencies may produce a stable interference fringe as long as the fringe movement caused by the beat waves is smaller than the fringe spacing during the pulse. Secondly, the pulses generated by the individual elements operating at slightly different frequencies may not emerge simultaneously. In order to phase lock short pulses, the laser beams of the elements need to be coherent in space and the pulses synchronized in time. Thus a more stringent requirement on frequency matching is need for the phase locking in the pulsed mode.

This chapter describes the operation of phase-locked monolithic Q-switched laser arrays using a low-Q Fourier-transform resonator. The monolithic Q-switched lasers are known to generate highly-stable single-transverse-mode and single-longitudinal-mode

pulses whose durations are in the several nanoseconds to 100 picoseconds range [41-43]. However, there is an inherent limitation on the pulse energy of a single device because of the onset of beam movement during the pulse as the cross-sectional area increases [53,54]. An effective technique of coherent combination of the power of a number of Q-switched lasers while maintaining the optical quality and short pulse duration is an important step toward power scaling of miniature solid-state lasers, including the microchip lasers and solid-state waveguide lasers which are subject to the same limitations in pulse energy.

6.2 Experimental

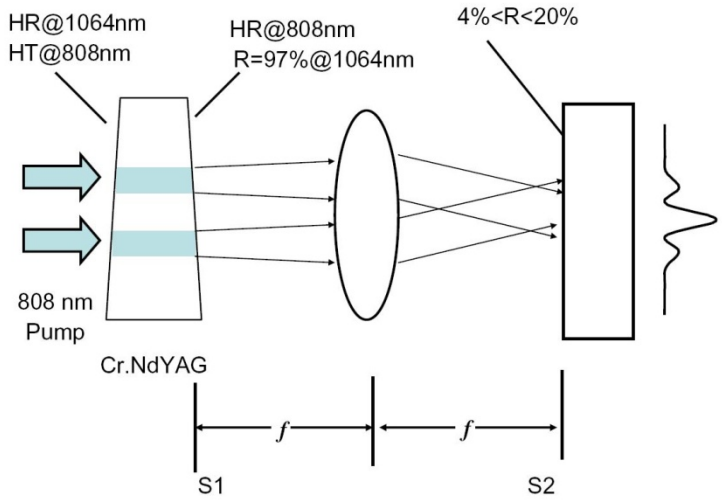

Fig. 6.1 Schematic of the phase locked Q-switched laser array.

The schematic of the phase locked Q-switched laser array is shown in Fig. 6.1. The Q-switched lasers are formed in a 2-mm-thick Cr^{4+}, Nd^{3+}:YAG crystal in which the Cr^{4+} ions act as the saturable absorbers [41-43]. The Nd^{3+} concentration is 1.1-wt%. The unsaturated absorption coefficient caused by the saturable absorber is 0.21 cm^{-1} at 1064 nm. The laser crystal is polished to form a flat–flat Fabry–Perot cavity. The pump facet is

coated for high transmission at 808 nm and high reflection at 1064 nm. The output facet is coated for 97% reflectivity at 1064 nm and high reflection at 808 nm to allow double passes of the pump beams within the gain medium. The lasers are end-pumped by diode laser beams through two optical fibers, each delivering 1.5Wat 808 nm. The pumping diodes are operated in the quasi-CW mode with a 300-μs pulse duration and at a repetition rate of 100 Hz. The diameter of the pumped region is 200 μm. The center-to-center separation between these two fibers is chosen to be 600 μm. At this separation, the far-field pattern when the two lasers are operating simultaneously is identical to those of the individual elements, indicating that the coupling between the lasers through the evanescent waves is negligible. The lasers are coupled to a Fourier-transform resonator which allows the relative phase of the laser elements to be stabilized by controlling the far-field pattern at the output mirror [30,55]. The output facet of the laser crystal is placed at one focal plane S1 of the converging lens and the output mirror is placed at the other focal plane S2. The focal length of the lens is 10 cm. A 1-cm thick etalon with a finesse of 60 at the lasing wavelength is used to analyze the lasing spectra. The beam profiles at the output mirror at S2 and the interference fringes after the etalon are monitored by two charge-coupled-device cameras. Three fast photodiodes with rise time less than 1 ns are used to detect the output of the individual elements and the combined output.

6.3 Results and discussion

In the absence of the optical feedback from the external resonator, the lasers generate Q-switched pulses in the TEM_{00} mode and a single longitudinal mode with pulse duration of 5.5 ns. The maximum output pulse energy is10 μJ per element. The combined

pulse energy from the two elements at the output is 20 μJ. The time series of the output exhibit two sets of pulse trains. The timing jitter of the pulses relative to the front edge of the pump pulse is on the order of 1 μs. Fig. 6.2(a) shows the beam profile at the output mirror of the free-running lasers which is the incoherent addition of the far-field profiles of the individual lasers. Due to a small deviation from perfect parallelism between the two end surfaces of the laser crystal, there exists a frequency mismatch between the lasers, which manifests itself as two sets of concentric fringes in the interferogram as viewed through the etalon. The frequency mismatch between the two lasers can be continuously controlled from zero to 1 GHz by rotating the crystal around the axis by 90 degrees. The resolution of the etalon is 160 MHz. Smaller frequency mismatches that cannot be resolvable by the etalon can be inferred from the angular position of the laser crystal measured from the position of zero frequency mismatches. From the maximum frequency mismatch and the center-to-center spacing of 600 μm, we estimate the maximum wedge angle between the end surfaces to be 7 seconds.

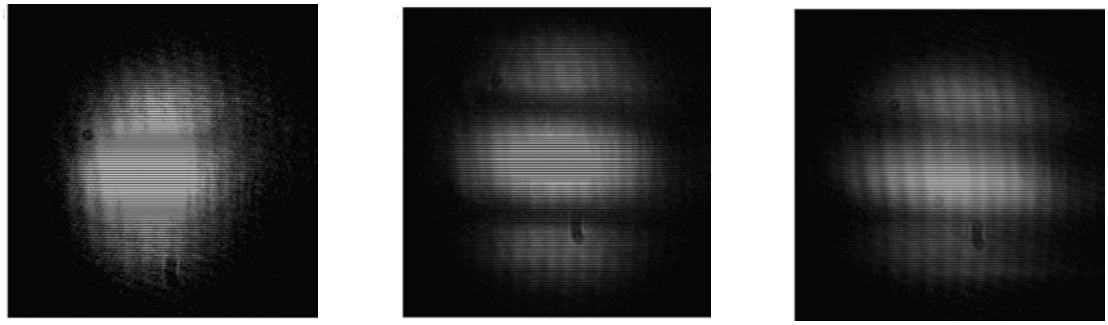

(a) (b) (c)

Fig. 6.2 Beam patterns of the two lasers operating (a) in the free-running state without the external resonator, (b) in the phase-locked state with zero frequency mismatch and (c) phase locked with a frequency mismatch of 20 MHz

When the external cavity is properly aligned and the frequency mismatch set to zero, the two lasers generate pulses with equal intensity and perfect coincidence. The

beam profile of at the output mirror S2 exhibits the interferential fringe pattern of either the in-phase or out-of-phase modes or irregularly switches between the two modes from shot to shot. The fringe spacing is 160 μm, which is consistent with that calculated from the separation of the two lasers and the focal length of the external resonator. To stabilize the phase relation, a single 20 μm-diameter wire is placed in front of the output mirror as the spatial filter to create a higher loss for the out-of-phase mode. With the filter in place, the contrast ratio of the fringe pattern increases dramatically and the pattern remains stationary. Fig. 6.2(b) shows the beam profile of the in-phase mode. The total output pulse energy of the phase-locked laser is 26 μJ, which is 30% higher than the total pulse energy of the two lasers in the free-running mode.

Fig. 6.3 shows the oscilloscope traces of the pulses from the individual elements. The relative time delay increases with increasing frequency mismatch. Fig. 6.3(a) shows that when the frequency mismatch is nearly zero, the two pulses coincide precisely in time. The two pulses become completely separated in time at $\Delta\nu$ = 50 MHz, as shown in Fig. 6.3(c). Fig. 6.3(d) shows the pulse pairs separated by 20 ns at $\Delta\nu$ = 300 MHz .With increasing frequency mismatch and decreasing optical feedback (by tilting and misaligning the external cavity mirror), a delay as large as 50 ns has been observed. We note that, while the pulses generated by the two elements in the free-running mode exhibit a large timing jitter on the order of a microsecond, the relative timing jitter between the pulse pair is zero.

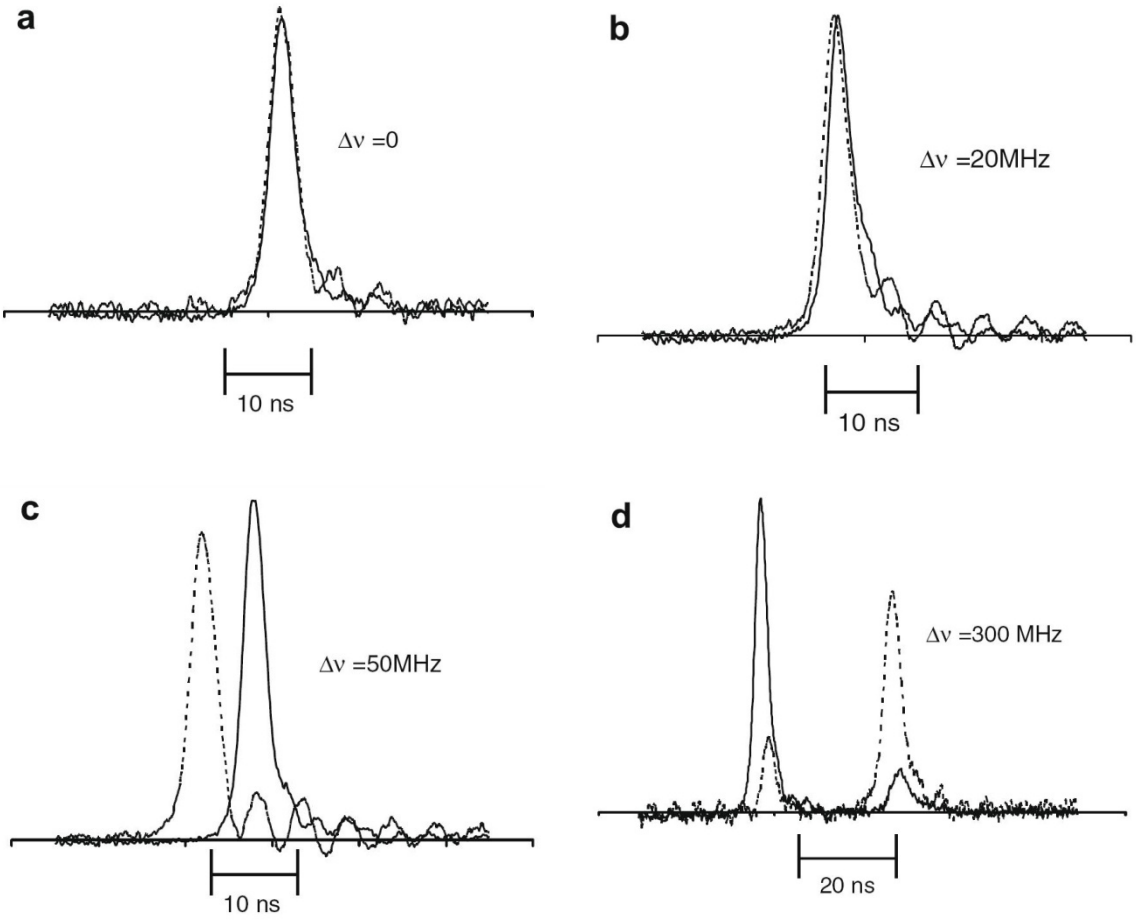

Fig. 6.3 Oscilloscope traces of phase-locked Q-switched pulses with (a) at zero frequency mismatch and (b) at frequency mismatches of 20 MHz, (c) 50 MHz, and (d) 300 MHz

As the frequency mismatch between the two elements increases, the fringe visibility at the output mirror gradually deteriorates. The combined output also successively exhibits pulse broadening, double pulsing, and complete separation of pulses as the frequency mismatch increases. The reduced fringe contrast and broadened pulses are due to the emergence of a relative time delay between the pulses from the individual elements. As an example, the far-field pattern of reduced contrast taken at $\Delta\nu = 20$ MHz is shown in Fig. 6.2(c). The corresponding oscilloscope traces of the pulses from individual elements are shown in Fig. 6.3(b).

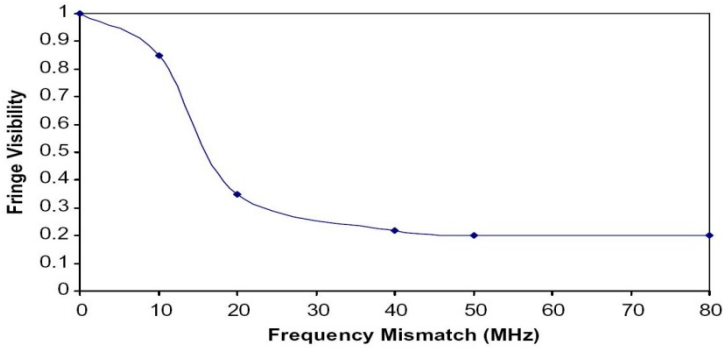

Fig. 6.4 Fringe visibility of the laser output as a function of frequency mismatch between the two lasing elements.

Fig. 6.4 shows the fringe visibility as a function of frequency mismatch between the two elements. When the frequency mismatch greater than 50 MHz, a poor fringe visibility of 0.2 is observed at the output mirror. A frequency mismatch of less than 20 MHz is desired to obtain good fringe visibility. To achieve a frequency mismatch of less than 20 MHz between two elements separated by 600 μm, the two planar surfaces of the laser crystal must be parallel to within 0.05 seconds, which is not achievable with standard polishing techniques. This stringent requirement of parallelism rules out the possibility of forming a two-dimensional phase-locked solid-state laser array in a single crystal, but still permits one-dimensional laser array to be formed along the direction of minimum wedge angle.

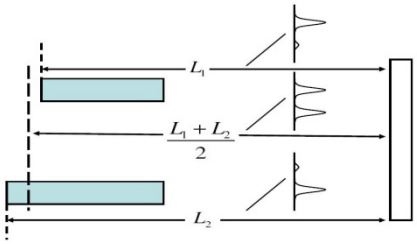

Fig. 6.5 Diagrams illustrating two lasers of unequal lengths coupled to a common external resonator and the intensity profiles of various spatial modes.

Multiple passes of the single pulses in the external resonator causes the laser pulses from the two lasing elements to be totally separated is caused by. The observed dynamics of the phase-locked mode and transition between the locked and unlocked states can be explained by the competition among the various eigenmodes in the laser array [56]. Although the passively Q-switched laser pulses are only 5 ns in duration, the process of laser intensity amplification from the initial spontaneous emission to the intensity level (which is strong enough to bleach the saturable absorber) is long. Thus the mode selection during the building-up period follows the same mechanism as in the continuous-wave lasers. We base our discussion on the model of two lasers of unequal lengths coupled to an external resonator as illustrated in Fig. 6.5. When the two elements have unequal lengths, the operating frequencies cannot satisfy the resonance conditions in both elements simultaneously and the modal profiles of the transverse modes are determined by the proximity of the frequencies to the various longitudinal modes. The symmetric modes, presumably resonant with the cavity whose length is the average of the two, generate two pulses of equal amplitudes in the individual elements simultaneously. However, the symmetric modes, being off resonance in both elements, are not favored unless the two elements are nearly equal in lengths. The dominating modes are expected to operate at the frequencies in the vicinity of the resonances of the individual elements. The spatial profiles of these modes are asymmetric with the stronger intensity residing in the element which is closer to resonance. The saturation of the saturable absorber further enhances the stronger element due to the reduced absorption loss caused by the stronger intensity. This process leads to the Q-switching pulse appearing in one of the elements first. The leading pulse then initiates the pulse in the other element, at a slightly different

center frequency, by the coupling through the external resonator. The coupling is an injection seeding process whose strength depends on the frequency mismatch relative to the spectral bandwidth of the laser pulse. When the resonance frequency of one of the elements falls within the spectral bandwidth of the laser, which is estimated to be 60 MHz, the coupling is strong and the relative time delay of the pulses can be smaller than the pulse duration. These partially overlapping pulses create a stable interference fringe but with reduced contrast ratio. When the frequency mismatch is larger than the spectral bandwidth, the coupling is weak and the trailing pulse can be totally separated from the leading pulse. Because of this interaction, the relative timing jitter is nearly zero even though the pulses are widely separated in time.

6.4 Conclusion

We have studied the effects of frequency mismatch on phase locking of two passively Q-switched lasers. Stable phase locking with a high degree of spatial coherence in the combined beam can be obtained when the frequency mismatch is less than the spectral linewidth of the laser pulses. As the frequency mismatch increases, the transition from the phase locked to the unlocked states is characterized by a gradual loss of coincidence of the pulses from the individual elements and a reduction in the fringe contrast. The observed phenomena can be explained by the dynamics of the asymmetric spatial modes in the laser array.

Chapter 7 Phase locking of Yb fiber lasers

7.1 Introduction

Fiber lasers are becoming the geometry of choice for high-power solid-state lasers because of proven advantages in compactness, efficiency, and beam quality. A single-mode fiber laser can produce an output of kilowatts [45]. The ultimate limitation of power from a single fiber laser is the onset of nonlinear effects such as stimulated Raman scattering and stimulated Brillouin scattering. Further increase in output power will require coherent addition of the outputs from multiple lasers in a laser array. Many researchers have studied beam combination in fiber laser arrays using various techniques, including interferometric addition in fiber couplers[57-61], the Talbot resonator[11,12,15-18], a self-organization mechanism in evanescent-coupled multicore fibers[9,10], and active phase correction[3-5].

From the phase control standpoint, the fiber laser arrays are different from diode laser arrays and solid-state (crystal) laser arrays [30,55,56], in their unequal and ever-changing path length among the fiber elements. The lengths of typical fiber lasers range from meters to tens of meters. It is practically impossible to ensure equal lengths among the elements. This is further complicated in the optical path lengths which are also constantly changing due to uncontrollable thermal and mechanical effects. An effective phase-locking technique must be able to respond to the changes and maintain a stable beam profile.

This chapter describes phase locking of two fiber laser array with arbitrary path lengths through a common Fourier transform resonator. The phase locked fiber laser array produces a diffraction-limited beam of the in-phase mode despite constant and

random changes in the optical path length in the individual elements. The ability to adapt to the changing environment is attributed to a self-adjusting process that can take place only in systems with a combination of long length, broad gain bandwidth, and low Q resonator, all of which can be found in fiber laser arrays. Yb doped silica fiber is characteristic of having broad gain bandwidth (from 975 nm to 1200 nm). Fibers with varying lengths have different free spectrum range. Resonance frequencies of the laser array must be a common multiple of the free spectral ranges of the fibers. When a relative phase change is introduced due to thermal and mechanical effects, the two sets of resonance frequencies will shift relative to each other and the original lasing frequency will no longer satisfy the boundary condition. The broad bandwidth provides thousands of possible longitudinal modes satisfying the condition of in-phase mode. Thus the laser array will respond to the phase change by switching to a slightly different frequency that satisfies the longitudinal and transverse boundary conditions.

7.2 Experimental

The schematic of the experimental setup is shown in Fig.7.1. Coherent beam combination of two fiber lasers is performed in a Fourier transform resonator, similar to the ones described in previous chapters. The resonator projects the far field patterns of the fiber emitters located at a focal plane S2 of a converging lens to the output mirror located at the other focal plane S3. When the waves from the emitters have the same phase, the far-field pattern is always simple with constructive interference occurring at zero degree. A matching spatial filter can be placed at the output mirror for mode selection.

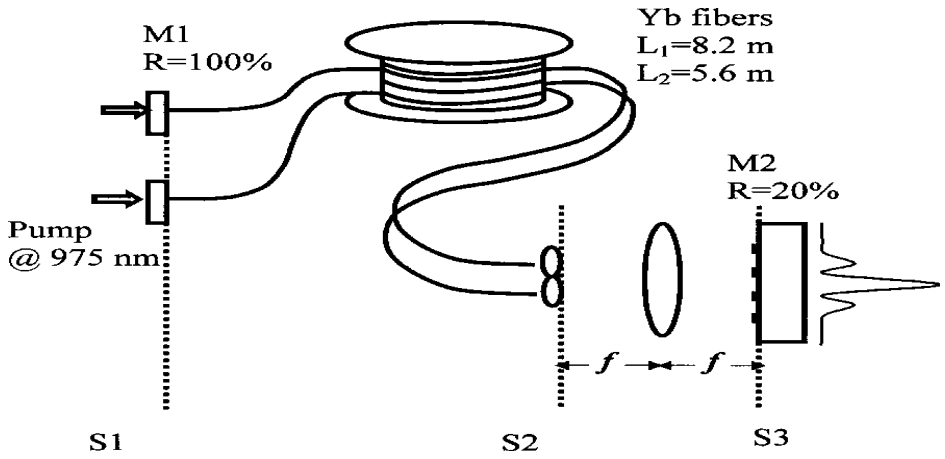

Fig. 7.1 Schematic of phase locking two fiber lasers

In the present study, the fiber gain media are the Nufern PM-YDF-5/125 double-clad ytterbium-doped fibers with a core diameter of 5-μm. The fiber lengths are 5.6 and 8.2 meters respectively. The nominal numerical aperture is 0.46 for the inner-cladding and 0.15 for the core. The small-signal absorption coefficient is 1.7 dB/m at 975 nm. The fiber lasers are end-pumped by two fiber-coupled laser diodes emitting at 972 nm wavelength. The fibers are terminated at S1 with a high reflectivity mirror centered at 1064 nm. The other ends are perpendicularly cleaved with 4% reflectivity. The beams from the fiber ends are expanded to a diameter of 3 mm. The collimated beams are positioned on the focal plane S2 of a converging lens. The center–to-center separation between the two beams is 1.1 cm. The output mirror with a reflectance of 22% at 1064 nm is placed at the other focal plane at S3. For the convenience of being able to construct the spatial filter using easily available thin metal wires, the focal length is chosen to be 40 cm. A single gold wire with a diameter of 12.75 micron as the spatial filter is placed in front of the output mirror to stabilize the phase relation. A charge-coupled device (CCD) camera and a laser beam analyzer are used to examine the beam profile of the output at

focal plane S3. And a radio-frequency spectrum analyzer is used to study the longitudinal mode spectra by analyzing the intensity fluctuations of laser output.

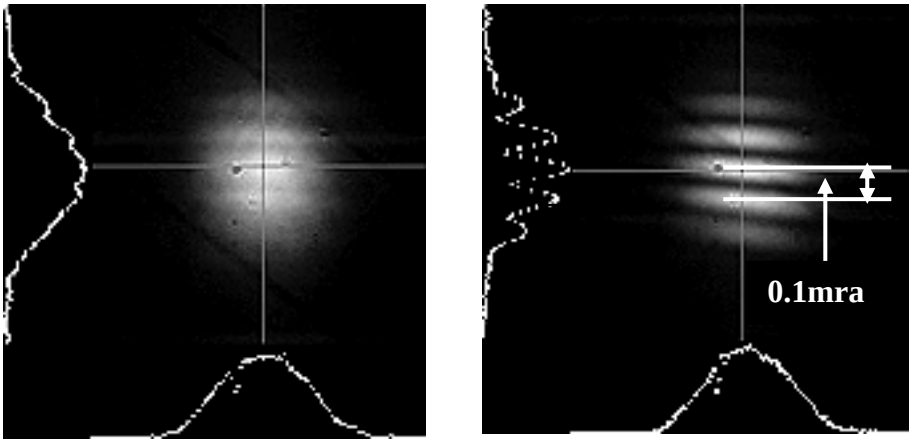

(a) (b)

Fig.7. 2 Beam patterns of fiber laser array in (a) free running (b) in-phase modes.

7.3 Results and discussion

With the aid of a CCD camera and a laser beam analyzer, we examine the beam profile of the output at focal plane S3. Fig. 7.2 (a) shows the beam profile at the output mirror of a free-running laser array without a spatial filter. The beam profile exhibits low-contrast interference fringes that are constantly moving with irregular pace and direction. The pace of fringe movement exacerbates and the contrast further degrades when the individual fibers are subject to mechanical perturbations. With the spatial filter moving in, it creates a higher loss for the out-of-phase mode and little loss to the in-phase mode. The 12.75-micron wire that we use in this experiment as a spatial filter creates 2.1% loss for the out-of-phase mode and 0.2% loss for the in-phase mode when placed at the third

intensity minimum of the in-phase mode. Better effect would be achieved with a thinner wire at the first intensity minimum of the in-phase mode. For example, a 5-micron wire at the first intensity minimum of the in-phase mode would introduce an 8% loss to the out-of-phase mode and 0.1% loss to the in-phase mode. But a 5 microns wire is not easy to handle and is subject to dramatic vibration from environment. When the wire is moved across the beam at the output mirror, the position of the intensity minimum simply follows that of the gold wire. Fig. 7.2 (b) shows the beam profiles of the in-phase. The small width-to-separation ratio of 3:11 of the collimated beams from the fiber emitters is limited by the available collimators, thus considerable fraction of the total energy is found in the side lobes. More energy can be concentrated in the central lobe by increasing the width of the individual beams relative to the separation or using a multicore fiber configuration.

With the spatial filter in place, the phase locking is stable even when the optical path lengths are deliberately changed. For example, no slight fringe movement is observed when the temperature of one of the fibers is raised by 20 ^{o}C, which changes the relative optical path length by at least 200 wavelengths. It appears that a self-adjusting process has taken place to adapt to the changing environment.

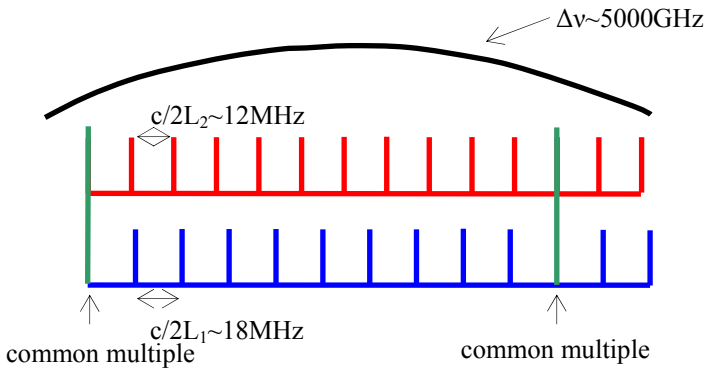

Fig.7.3 Common multiple of two fiber lasers' frequencies.

The self-adjusting process can be understood in terms of selection of common resonances in a compound resonator [56-59]. The position of the spatial filter at the output mirror dictates the relative phase in the laser array. As shown in Fig. 7.3, the resonance frequencies of the waves in the fiber laser array, with individual length L_1 and L_2, must simultaneously satisfy the boundary conditions of having nodes at plane S1 and having the same phase at S2. Thus the lasing frequencies are characterized by the common multiples of the free spectral ranges $c/(2nL_1)$ and $c/(2nL_2)$ of the individual fiber lasers. When the optical path length of one of the element changes, a new set of common resonances slightly shifted from original longitudinal modes must emerge. This self-adjusting process is not always possible, but works the best in laser systems with a combination of broad gain bandwidth, long and unequal lengths, and low-Q resonator. The broad bandwidth and long lengths provide a large number of closely-spaced longitudinal modes within the gain bandwidth, making it easier to find common resonances. The low-Q values of the resonator broaden the resonance lines to allow those near the commonly resonance to overlap. In the present case, there are 10^5 longitudinal modes within the gain bandwidth of the fiber laser with 5- meter length. The fiber resonators with 100% and 4% reflectance at the end mirrors have a finesse value of 2. Thus all of the favored conditions can be met in fiber lasers.

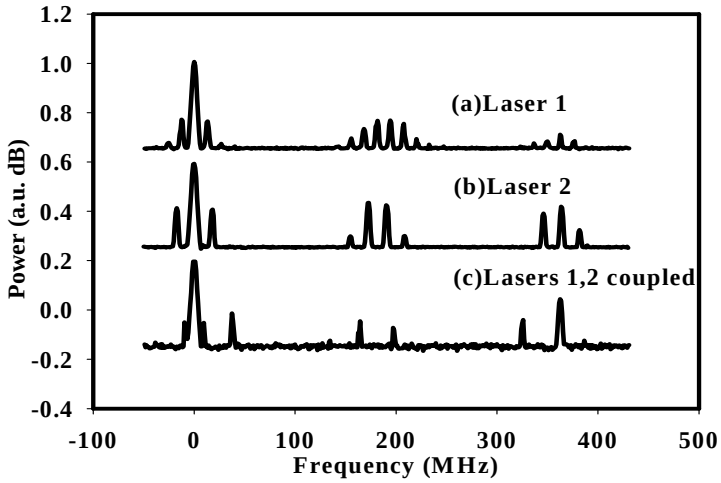

Fig.7.4 Spectra of intensity fluctuations of individual and phase locked fiber lasers

To study the longitudinal mode spectra, we analyzed the intensity fluctuations of laser output using a radio-frequency spectrum analyzer. First, we align the output mirror to decouple the two fiber lasers. The spectra of the beat waves of the individual lasers, shown in Fig. 7.4 (a) and (b), consist of equally-spaced peaks with an envelope modulation of 180 MHz, which is caused by the 0.8-m-long external cavity. The beat frequency of 12.53 MHz and 18.35 MHz are the free spectral ranges of the fiber lasers of length L_1=8.2 meters and L_2= 5.6 meters respectively. When the output mirror is aligned to create the phase-locked mode, the spectrum of the beat waves exhibits fewer peaks at 38 MHz and its multiples at 153 MHz and 198 MHz, respectively. In the present coupled system with a length difference of L = 2.6 m, the minimum common multiple is predicted to be $\Delta\nu = c/(2n\Delta L) = 39MHz$, which is consistent with the observed value of 38 MHz.

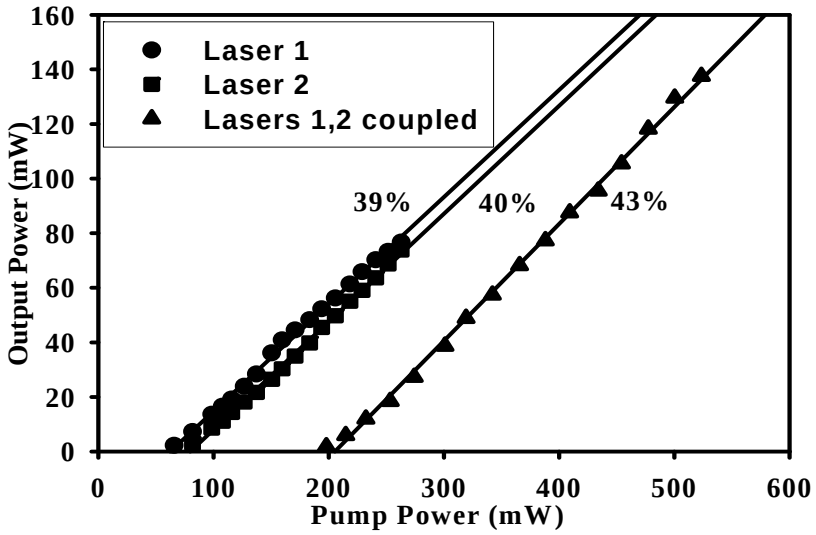

Fig. 7.5 Output vs. pump power relation of the laser array and the individual fiber lasers.

Fig. 7.5 shows the measured output vs. pump power relation of the individual fiber lasers and for the phase locked array operating in the in-phase mode. The slope efficiencies are 39 %, and 40 % for laser 1 and laser 2, respectively, and 43 % for the phase locked mode. The efficiency of coherent power combination is 92% for a pump power of 600 mW.

7.4 Conclusion

In conclusion, we have successfully phase-locked two fiber lasers with un-equal and varying optical path lengths with high efficiency. The stable phase locking is attributed to a self-adjusting process by which the laser array prefers to operate in common resonance frequencies of the composite system. This is mainly due to the specific virtues of fiber lasers of having long length, broad bandwidth and low Q-resonance. This study suggests that it may be possible to phase lock of a large number of fiber lasers without the needs for active phase control.

Chapter 8 Phase locking of SBS Q-switched pulses

8.1 Introduction

With various methods of active or passive Q switching, fiber lasers can be used for generating pulses with durations which are typically between hundreds of nanoseconds and tens of microseconds [62-64]. As fiber lasers typically have relatively long resonators, the pulse durations tend to be longer than those of bulk lasers. The pulse energy achievable with large mode area fibers can be several millijoules, and is essentially limited by the saturation energy and by the damage threshold, especially for shorter pulses. Coherent coupling of several pulsed fiber lasers to achieve a high-peak-power pulse is of interest for various applications, including medicine, remote sensing, and nonlinear optical processes.

Recently, there have been reports of using Brillouin backscattering as a distributed passive *Q*-switching mechanism to generate short pulses of 2–5 ns duration that are much shorter than the resonator lengths[65-68]. Unlike the conventional *Q*-switching fiber lasers, in which the pulse duration is proportional to the photon lifetime in the resonator, the short pulses generated by stimulated Brillouin scattering (SBS) do not depend on the photon lifetime in the resonator but rather on the dynamics of the nonlinear process. Short pulse generation through SBS in fiber lasers can be a self-starting process that does not require an intracavity modulator, but the occurrence of pulses was found to be highly irregular in pulse energy, shape, and repetition rates [66,68]. There have been reports of pulse stabilization using an acousto-optic modulator [65] and Cr^{4+}:YAG saturable absorber [68]. The phase locking of short laser pulses generated by the

nonlinear processes, whose development is stochastic, faces the challenge of having to ensure that the short pulses are initiated simultaneously. There is also a question of whether the relative phase of laser pulses generated by a high-gain nonlinear process with a frequency shift from the primary laser can be effectively controlled by the same mechanism of phase locking in the resonator of the primary laser.

This chapter describes the phase locking operation of intense short pulses generated by stimulated Brillouin backscattering in two Yb-doped double-clad fiber lasers. The phase locking of two fiber lasers is achieved through interaction with a self-induced loss modulation in a saturable absorber, which also plays the role of initiating and stabilizing the *Q*-switched pulses.

8.2 Experimental

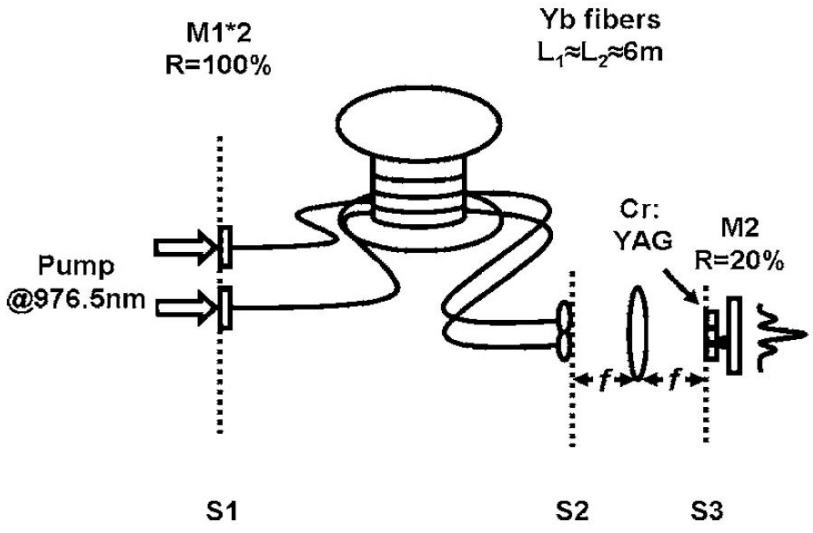

Fig. 8.1 Experimental setup of phase locking SBS Q-switched pulses

The schematic of the experiment setup as shown in Fig. 8.1 is similar to the ones used previously to phase lock one- and two-dimensional laser arrays of fixed lengths described in Chapter 5, 6, and 7. The fiber gain media are two Nufern PM-YDF-5/125 double-clad ytterbium-doped fibers with a core diameter of 5 μm. The numerical aperture is 0.46 for the inner cladding and 0.15 for the core. The two fibers are approximately 6 m long. The small-signal absorption is 1.7 dB/m at 975 nm. The resonator mirrors at the pump end have high transmission at 976 nm and total reflection at 1064 nm. The other ends are angle cleaved at 8° to suppress the optical feedback from the fiber ends. The beams from the fibers are expanded to 3 mm diameter and coupled to a Fourier transform resonator. A 1-mm-thick Cr:YAG saturable absorber with an unsaturated transmission of 50% at 1064 nm is placed in front of the output mirror to induce *Q*-switched pulses. And a single gold wire with a diameter of 12.5 micron as the spatial filter is placed in front of the output mirror to stabilize the phase relation.

8.3 Results and discussion

The pump diode lasers are operated in the quasi-continuous-wave mode with 700 μs duration and 60 Hz repetition rate. When the pump power reaches the threshold of 0.5 W in each fiber laser, a train of *Q*-switched pulses is observed. The pulse duration is 1 μs and the pulse energy stays nearly constant as the pump power increases. With the aid of a charge-coupled device camera and a laser beam analyzer, we examined the beam profile of the output at focal plane S3. The beam profile exhibits low-contrast interference fringes that are constantly moving from pulse to pulse. The fringe spacing is 18 μm. When the gold wire is placed in front of the output mirror along one of the dark fringes of

the in-phase mode as the spatial filter, it creates a higher loss for the out-of-phase mode and little loss to the in-phase mode. The fiber laser array exhibits stable phase locking in in-phase mode. Such beam profile is shown as Fig. 8.2(a)

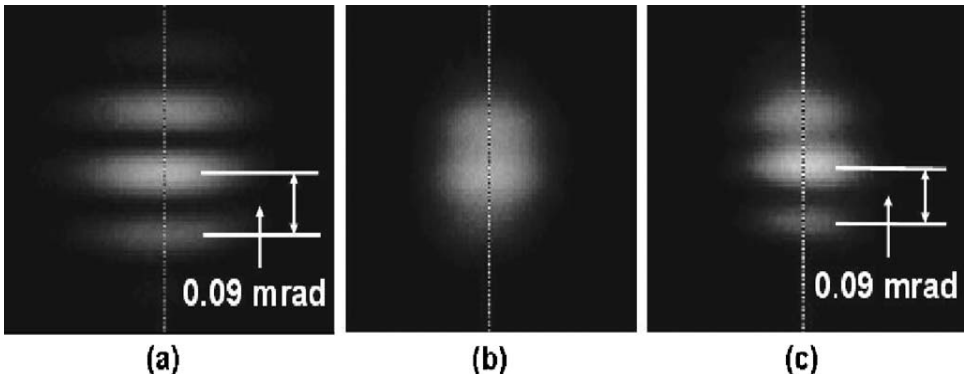

Fig. 8.2 Beam profiles at the output mirror of (a) phase-locked *Q*-switched laser pulses, (b) free-running SBS pulses, and (c) phase-locked SBS pulses.

When the output mirror is slightly misaligned from its optimal position, the lasing threshold steadily increases with the misalignment and *Q*-switched pulses evolve into a train of intense pulses of 1.5 ns pulse duration and much higher pulse energy. The development of the short pulse is attributed to the onset of SBS, which creates a traveling high reflector in the fibers and thereby depletes the energy stored in the gain media through *Q* switching. The intense SBS pulses have ten times the pulse energy and much shorter pulse duration of the long *Q*-switched pulses that initiate them. With arbitrarily chosen fiber lengths, the giant pulses from the two fiber lasers generally are not phase locked and the beam profile at the output mirror exhibits poor contrast ratio, as shown in Fig. 8.2(b) The pulses from the individual fibers appear to be generated independent from each other and therefore do not overlap in time, as shown in Fig. 8.3(a).The interference fringes are stabilized when the difference in lengths of the two fiber resonators is less

than 2 cm. Fig. 8.2(c) shows the beam profile at the output mirror when the two lasers are operated in phase.

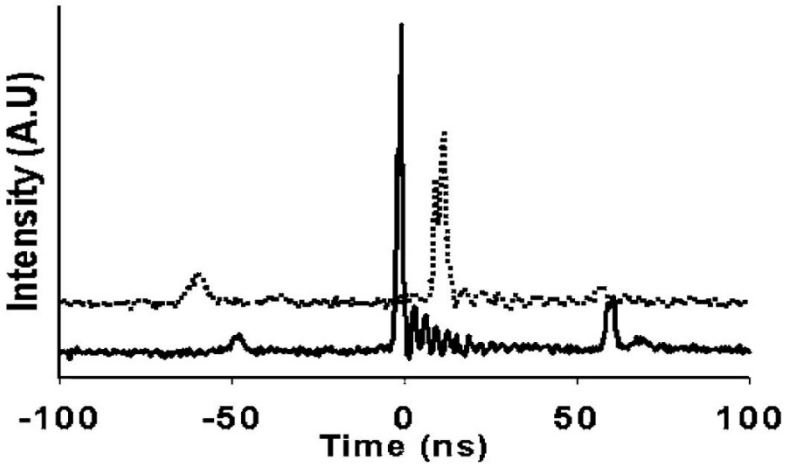

(a)

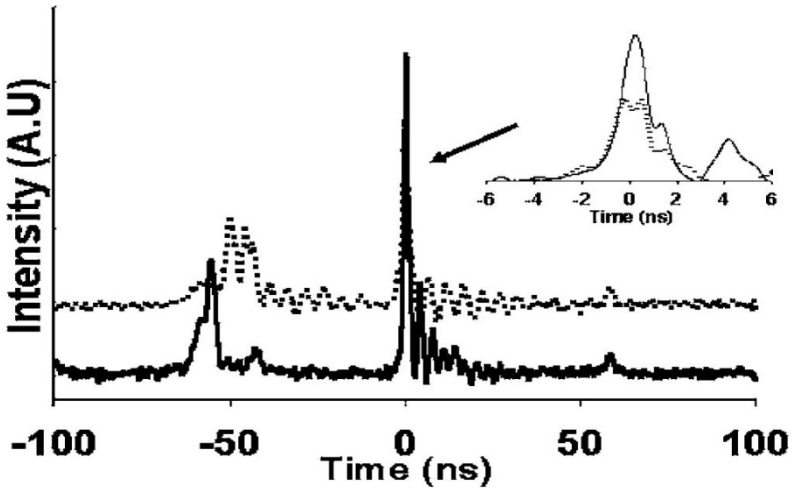

(b)

Fig.8.3 Oscilloscope traces of the laser pulses from two fiber lasers when they are phase (a) unlocked and (b) locked.

The time series of the oscilloscope traces also confirms the coincidence of pulses from pulses from the individual lasers, as shown in Fig. 8.3(b). The time series of the output power also shows that the pulse duration in the final stage of development leading to the strongest pulse is much shorter than the round-trip time. The round-trip

amplification is about 10. Thus a two-element laser system is essentially a two-armed laser amplifier for free-propagating pulses during the final stage. Any unevenness in the waveguide and pump level can result in unbalanced output pulse energy from each fiber. This explains the lower contrast ratio of the beam profile at the output mirror, compared to those for the conventional *Q*-switched laser pulses.

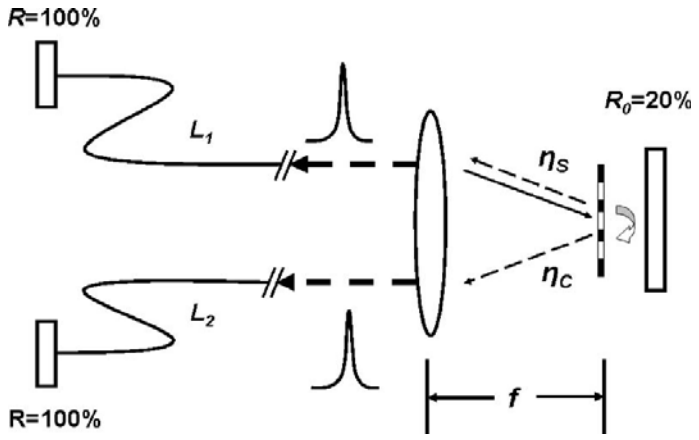

Fig.8.4 Two-element laser coupled through a diffractive element in an external resonator

Based on the experimental results, we can describe the mechanism by which the phase-locked stimulated Brillouin pulses are generated in the two-element fiber laser array. At the beginning of the cycle, a passively *Q*-switched pulse is generated due to the action of the saturable absorption in Cr:YAG. The interference fringes at the output mirror created by the leading edge of the *Q*-switched pulse bleach the Cr:YAG crystal and establish a loss grating which provides the diffractive optical feedback for the individual fiber lasers and cross coupling between the lasers. The diffractive feedback has a self-coupling efficiency η_S, and a cross coupling efficiency η_C, as illustrated in Fig. 8.4. When the intensity of the conventional *Q*-switched laser pulses is high enough to trigger the SBS process, a frequency shifted seed pulse is generated. In a two-element fiber laser

array with lengths $L1$ and $L2$ coupled to an external resonator, there are three resonators with gain lengths $L1$, $L2$, and $L1+L2$, sharing the common gain media. In the absence of the self-coupling η_S, the resonator with length $L1+L2$ has the largest gain length and the lowest threshold for the SBS process. The SBS pulses thus created would be propagating in the two fibers sequentially and the output from the fibers cannot be phase locked. In the present experiment, the first order diffraction of the loss grating in the saturable absorber provides a self-coupling strength of approximately 30% and cross coupling strength of 70%, assuming a full saturation of the saturable loss. This enables the SBS pulses initiated in one of the arms of the gain media to become the seeds for amplification in both arms of the gain medium simultaneously and their interaction through the diffractive element in the common external resonator can result in-phase locking. Since the pulse duration of the SBS pulses is much shorter than the round-trip time in the individual resonator, effective phase locking also requires that the difference in fiber lengths be much less than the pulse duration.

In the present study, the combined peak power is 6.67 kW, corresponding to a power density of 17 GW/cm^2 in each fiber. Further increase in pulse energy in each fiber laser, achievable by increasing the energy storage in a lower-Q resonator, results in optical damage in the fiber ends. The pulse energy of the phase-locked mode for the coherently combined pulses is 10 μJ, which is two times the pulse energy of the individual fiber lasers. The efficiency of the coherent beam combination is high. This points to the possibility of a coherent combination of intense laser pulses generated by nonlinear processes in multiple fiber lasers to achieve higher brightness much beyond the power density of optical damage of a single fiber.

8.4 Conclusion

In conclusion, we have demonstrated phase-locked operation of the output of two Brillouin backscattering *Q*-switched fiber lasers whose pulse durations are much shorter than the round-trip time of the resonators. Despite the stochastic nature in the dynamics of nonlinearity, simultaneous generation and phase locking of short pulses have been achieved through diffractive coupling and spatial filtering in an external Fourier-transform resonator.

Chapter 9 Summary

In this thesis project, we have investigated and demonstrated phase locking in laser arrays of various configurations, including a monolithic 2x2 Nd:VVO_4 array, a two-element Q-switched laser array, a two-element fiber laser array operating in continuous-wave mode, and a two-element Brillouin scattering Q-switched fiber laser array. The elements in the arrays are coherently coupled through a common Fourier-transform resonator. In the resonator, the far-field pattern of the emitters is projected to the output mirror by a converging lens. Mode selection is done by placing a simple spatial filter that matches the beam profile of the in-phase mode at the output mirror. We have succeeded in achieving highly stable in-phase operation in continuous-wave laser arrays.

In short-pulse Q-switched laser arrays, the phase-locked operation requires tight control of the path lengths of the individual element to ensure the pulses generated by the individual elements overlap in time. Typically, a leading pulse first emerges from the element having the lowest cavity loss. The leading pulse then initiates the laser action in the other element, at a slightly different center frequency through injection seeding whose strength depends on the frequency mismatch relative to the spectral bandwidth of the laser pulse. When the resonance frequency of one of the elements falls within the spectral bandwidth of the other, the coupling is strong and the relative time delay of the leading and trailing pulses can be smaller than the pulse duration. These partially overlapping pulses create a stable interference fringe but with reduced fringe contrast. When the frequency mismatch is larger than the spectral bandwidth, the coupling is weak and the trailing pulse can be totally separated from the leading pulse, and the pulses are temporally coherent but spatially incoherent.

Our study has proven the feasibility of using a Fourier-transform resonator to phase lock solid-state laser arrays. The method has many advantages over the more elaborate schemes in its simplicity, high efficiency, versatility, and reliability.

Since the concept has been proven, further study could lie in two directions. One is to scale the laser array to a large number of elements, and the other is to miniaturize resonator by using the two end surfaces of a quarter-pitch graded-index lens to form the Fourier-transform resonator. The miniature resonator can find applications in phase locking of a bundle of fiber lasers or multicore fiber laser arrays.

Bibliography

1. T. Y. Fan, “Laser beam combining for high-power, high-radiance sources”, IEEE J. Sel. Top. Quantum Electron. 11 (3), 567 (2005).

2. J. S. Osinski, D. Mehuys, D. F. Welch, R. G. Waarts, J. S. Major, Jr., K. M. Dzurko, and R. J. Lang, “Phased array of high-power, coherent, monolithic flared amplifier master oscillator power amplifiers”, Appl. Phys. Lett. 66, 556 (1995).

3. J. Anderegg, S. Brosnan,M. Weber, H. Komine, and M. Wickham, “8-W coherently phased 4-element fiber array, ” Proc. SPIE,vol. 4974, pp. 1-6, 2003.

4. S. J. Augst, T. Y. Fan, and A. Sanchez, “Coherent beam combining and phase noise measurements of ytterbium fiber amplifiers”, Opt. Lett. 29 (5), 474 (2004).

5. T. M. Shay, V. Benham, J. T. Baker, A. D. Sanchez, D. Pilkington, and C. A. Lu, "Self-Synchronous and Self-Referenced Coherent Beam Combination for Large Optical Arrays," IEEE J. Sel. Top. Quantum Electron. 13, 480-486 (2007).

6. D. G. Youmans, “Phase locking of adjacent channel leaky waveguide CO_2 lasers”, Appl. Phys. Lett. 44, 365 (1984).

7. L. J. Mawst, D. Botez, C. Zmudzinski, M. Jansen, C. Tu, T. J. Roth, and J. Yun, “Resonant self-aligned-stripe antiguided diode laser array”, Appl. Phys. Lett. 60, 668 (1992).

8. S. Sanders, R. Waarts, D. Nam, D. Welch, D. Scifres, J. C. Ehlert, W. J. Cassarly, J. M. Finlan and K. M. Flood, “High power coherent two-dimensional semiconductor laser array”, Appl. Phys. Lett. 64, 1478 (1994).

9. E. J. Bochove, P. K. Cheo, and G. G. King, "Self-organization in a multicore fiber laser array," Opt. Lett. 28, 1200-1202 (2003).

10. Y. Huo, P. Cheo, and G.King, "Fundamental mode operation of a 19-core phase-locked Yb-doped fiber amplifier," Opt. Express 12, 6230-6239 (2004).

11. L. Michaille, C. R. Bennett, D. M. Taylor, T. J. Shepherd, J. Broeng, H. R. Simonsen, and A. Petersson, "Phase locking and supermode selection in multicore photonic crystal fiber lasers with a large doped area," Opt. Lett. 30, 1668-1670 (2005).

12. L. Li, A. Schülzgen, S. Chen, V. L. Temyanko, J. V. Moloney, and N. Peyghambarian, "Phase locking and in-phase supermode selection in monolithic multicore fiber lasers," Opt. Lett. 31, 2577-2579 (2006).

13. J. R. Leger, M. L. Scott, and W. B. Veldkamp, “Coherent addition of AlGaAs lasers using microlenses and diffractive coupling”, Appl. Phys. Lett. 52,1771 (1988).

14. R. Waarts, D. Mehuys, D. Nam, D. Welch, W. Streifer, and D. Scifres," High-power, cw, diffraction-limited, GaAlAs laser diode array in an external Talbot cavity ", Appl. Phys. Lett. 58, 2586 (1991).

15. M. Wrage, P. Glas, D. Fischer, M. Leitner, D. V. Vysotsky, and A. P. Napartovich, "Phase locking in a multicore fiber laser by means of a Talbot resonator," Opt. Lett. 25, 1436-1438 (2000).

16. M. Wrage, P. Glas, and M. Leitner, "Combined phase locking and beam shaping of a multicore fiber laser by structured mirrors," Opt. Lett. 26, 980-982 (2001).

17. M. Wrage, P. Glas, D. Fisher, M. Leitner, N.N. Elkin, D.V. Vysotsky, A.P. Napartovich, and V.N. Troshchieva, “Phase-locking of a multicore fiber laser by wave propagating through an annulawaveguide”, Opt. Commun. 205, 367 (2002).

18. M. Valley, G. Lombardi, and R. Aprahamian, "Beam combination by stimulated Brillouin scattering," Optical Society of America, Journal, B: Optical Physics 3, 1492-1497 (1986).

19. N. G. Basov, I. G. Zubarev,A. B. Mironov, S. I. Michailov, A.Yu.Okulov, "Phase fluctuations of the Stockes wave produced as a result of stimulated scattering of light". Sov.Phys. JETP Lett.,v.31,p.645(1980).

20. D. A. Rockwell, and C. R. Giuliano, "Coherent coupling of laser gain media using phase conjugation," Optics Letters 11, 147-149 (1986).

21. R. H. Moyer, "Beam combination with stimulated Brillouin scattering: A review," SPIE Conference on Laser Wavefront Control, 25-32 (1988).

22. D. L. Carroll, R. Johnson, S. J. Pfeifer, and R. H. Moyer, "Experimental investigations of stimulated Brillouin scattering beam combination," J. Opt. Soc. Amer. B 9, 2214–2224 (1992).

23. D. S. Sumida, D. C. Jones, and D. A. Rockwell, "An 8.2 J phase-conjugate solid-state laser coherently combining eight parallel amplifiers," Quantum Electronics, IEEE Journal of 30, 2617-2627 (1994).

24. H. Becht, "Experimental investigation on phase locking of two Nd: YAG laser beams by stimulated Brillouin scattering," J Opt Soc Am B 15, 16-78 (1998).

25. J. Falk, M. Kanefsky, and P. Suni, "Limits to the efficiency of beam combination by stimulated Brillouin scattering," Opt. Lett 13, 39–41 (1988).

26. S. Sternklar, D. Chomsky, S. Jackel, and A. Zigler, "Misalignment sensitivity of beam combining by stimulated Brillouin scattering," Opt. Lett. 15, 469-470 (1990).

27. R. Moyer, M. Valley, and M. Cimolino, "Beam combination through stimulated Brillouin scattering," Optical Society of America, Journal, B: Optical Physics 5, 2473-2489 (1988).

28. N. F. Andreev, E. A. Khazanov, O. V. Kulagin, B. Z. Movshevich, O. V. Palashov, G. A. Pasmanik, V. I. Rodchenkov, S. Scott, and P. Soan, "A two-channel repetitively pulsed Nd: YAG laser operating at 25 Hz with diffraction-limited beam quality," IEEE Journal of Quantum Electronics 35, 110-114 (1999).

29. G. T. Moore, "A model for diffraction-limited high-power multimode fiber amplifiers using seeded stimulated Brillouin scattering phase conjugation," IEEE Journal of Quantum Electronics 3**7**, 781 (2001).

30. S. Ménard, M. Vampouille, B. Colombeau, and C. Froehly, "Highly efficient phase locking and extracavity coherent combination of two diode-pumped Nd:YAG laser beams," Opt. Lett. 21, 1996-1998 (1996).

31. J. K. Butler, D. E. Ackley, and D. Botez, "Coupled-mode analysis of phase-locked injection laser arrays," Appl. Phys. Lett. 44**,** 293-295 (1984); Appl. Phys. Lett. 44**,** 935 (erratum) (1984).

32. T. L. Paoli, W. Streifer, and R.D. Burnham. "Observation of Supermodes in a Phase-locked Diode Laser Array," Appl. Phys. Lett. 45: 217-219 (August,1984).

33. J. E. Epler, N. Holonyak, R. D. Burnham, T. L. Paoli, and W. Streifer "Far-field Supermode Patterns of a Multi-stripe Quantum Well Heterostructure Laser Operated in an External Grating Cavity," Appl. Phys. Lett. 45: 406-408 (August 1984).

34. E. Kapon, J. Katz, and A. Yariv, "Supermode analysis of phase-locked arrays of semiconductor lasers," Opt. Lett. 9, 125-127 (1984); Opt. Lett. 9, 318-318 (erratum) (1984).

35. S. R. Chinn and R. J. Spiers, "Modal gain in coupled-stripe lasers",IEEE J. Quantum Electron.QE-20, 358 (1984).

36. D. Botez, "Array-Mode Far-Field Patterns for Phase-Locked Diode-Laser Arrays: Coupled-Mode Theory Versus Simple Diffraction Theory," IEEE J. Quantum Electron., Vol. QE-21,pp. 1752-1755, November 1985.

37. M. Segev, and B. Fischer. "Laser Diode Arrays with Apertured Phase Conjugate Feedback," IEEE Journal of Quantum Electronics*,* 26 (8): 1318-1322 (August,1990).

38. D. R. Scifres, R. D. Burnham, and W. Streifer. "Phase Locked Semiconductor Laser Array," Applied Physics Letters*,* 33: 1015-1017 (1978).

39. R. R. Drenten, "waveguiding aspects of advanced semiconductor lasers and miniature blue-green lasers", Thesis ,(1996), Chap. 4.

40. W. Koechner: *Solid-State Laser Engineering* (Springer, Berlin, 1999) 5th ed., Springer Series in Optical Sciences, Vol. 1.

41. S. Zhou, K.K. Lee, Y.C. Chen and S. Li, "Monolithic self-Q-switched Cr,Nd:YAG laser", Opt. Lett. 18, 511 (1993).

42. S. Li, S. Zhou, P. Wang, Y. C. Chen, and K. K. Lee, "Self-Q-switched diode-end-pumped Cr,Nd:YAG laser with polarized output," Opt. Lett. 18, 203- (1993).

43. J. Dong, P. Deng, Y. Lu, Y. Zhang, Y. Liu, J. Xu, and W. Chen, "Laser-diode-pumped Cr^4+, Nd^3+:YAG with self-*Q*-switched laser output of 1.4 W," Opt. Lett. 25, 1101-1103 (2000).

44. A. Liu, K. Ueda, "The absorption characteristics of circular, offset, and rectangular double-clad fibers," Opt. Comm., Vol. 132, 511-518, (1996).

45. Y. Jeong, J. Sahu, D. Payne, and J. Nilsson, "Ytterbium-doped large-core fiber laser with 1.36 kW continuous-wave output power," Opt. Exp. 12, 6088-6092 (2004).

46. M. J. F. Digonnet, Rare-earth-doped fiber lasers and amplifiers, 2nd edition, Marcel Dekker, Inc., New York, 2001.

47. V. Gapontsev, D. Gapontsev, N. Platonov, O. Shkurkhin, V. Fomin, A. Mashkin, M. Abramov, and S.Ferin, "2 kW CW ytterbium fiber laser with record diffraction limited brightness," in Proceedings of theConference on Lasers and Electro-Optics Europe, (Optical Society of America, 2005) (Note: Used 14μmMFD fiber implying 13W/μm2 power handling capability without damage.)

48. A. Galvanauskas, Z. Sartania, and M. Bischoff, " Millijoule femtosecond fiber CPA system," in Advanced Solid-State Lasers, C. Marshall, ed., Vol. 50 of OSA Trends in Optics and Photonics (Optical Society of America, 2001), paper PD3.

49. J. Nilsson, J. K. Sahu, Y. Jeong, W. A. Clarkson, R. Selvas, A. B. Grudinin, S. Alam, "High Power Fiber Lasers:New Developments," Advances in Fiber Devices, Proceedings of SPIE, Vol. 4974, (2003).

50. H. M. Pask, R. J. Carman, D. C. Hanna, A. C. Tropper, C. J. Mackechnie, P. R. Barber, J. M. Dawes, "Ytterbium-Doped Silica Fiber Lasers: Versatile Sources for the 1-1.2 μ m Region," IEEE J. Sel. Top. Quantum Electron. 1, 2-13 (1995).

51. R. W. Boyd, nonlinear optics, (Academic Press, San Diego, 1992), Chap. 8,9.

52. G. P. Agrawal, Nonlinear Fiber Optics, 3rd ed. (Academic Press, 2001).

53. G. Yao, S. Zhou, P. Wang, K. K. Lee, and Y.C. Chen, "Dynamic of transverse mode in self-Q-switched solid-state lasers", Opt. Commun. 114, 101-104 (1995).

54. H. Liu, S. Zhou, and Y. C. Chen, "High-power monolithic unstable-resonator solid-state laser," Opt. Lett. 23, 451-453 (1998).

55. Y. Zhou, L. Liu, C. Etson, Y. Abranyos, A. Padilla, and Y.C. Chen, "Phase locking of a two-dimensional laser array by controlling the far field pattern", Appl. Phys. Lett., 84, 3025 (2004).

56. J. Xu, K.K. Lee, and Y.C. Chen, "Phase locking in a two-element laser array with detuning" Opt. Commun. 117 , 198-126 (1995).

57. V. A. Kozlov, J. Hernández-Cordero, and T. F. Morse, "All-fiber coherent beam combining of fiber lasers," Opt. Lett. 24, 1814-1816 (1999).

58. T. Simpson, A. Gavrielides, and Phillip Peterson, "Extraction characteristics of a dual fiber compound cavity," Opt. Express 10, 1060-1073 (2002).

59. D. Sabourdy, V. Kermene, A. Desfarges-Berthelemot, L. Lefort, A. Barthelemy, C. Mahodaux, and D. Pureur, "Power scaling of fiber lasers with all-fiber interferometric cavity," Electron. Lett. 38, 692-693 (2002).

60. D. Sabourdy, V. Kermene, A. D. Berthelemot, L. Lefort, A. Barthelemy, P. Even, and D. Pureur, "Efficient coherent combining of widely tunable fiber lasers," Opt. Express 11, 87-97 (2003).

61. A. Shirakawa, T. Saitou, T. Sekiguchi, and K. Ueda, "Coherent addition of fiber lasers by use of a fiber coupler," Opt. Express 10, 1167-1172 (2002).

62. C.C. Renaud, R.S. Selvas-Aguilar, J. Nilsson, P.W. Turner, A.B. Grudinin, " Compact high-energy Q-switched cladding-pumped fiber laser with a tuning range over 40 nm", IEEE Phot. Tech. Lett. 11, 976 (1999).

63. P. Petropoulos, H. L. Offerhaus, D. J. Richardson, S. Dhanjal, and N. I. Zheludev, "Passive Q-switching of fiber lasers using a broadband liquefying gallium mirror", Appl. Phys. Lett. 74, 3619 (1999).

64. M. Laroche, A. M. Chardon, J. Nilsson, D. P. Shepherd, W. A. Clarkson, S. Girard, and R. Moncorgé, "Compact diode-pumped passively *Q*-switched tunable Er-Yb double-clad fiber laser," Opt. Lett. 27, 1980-1982 (2002).

65. Z. J. Chen, A. B. Grudinin, J. Porta, and J. D. Minelly, "Enhanced *Q* switching in double-clad fiber lasers," Opt. Lett. 23, 454-456 (1998).

66. Mohammed Salhi, Ammar Hideur, Thierry Chartier, Marc Brunel, Gilles Martel, Cafer Ozkul, and François Sanchez, "Evidence of Brillouin scattering in an ytterbium-doped double-clad fiber laser," Opt. Lett. 27, 1294-1296 (2002).

67. Ya-Xian Fan, Fu-Yun Lu, Shu-Ling Hu, Ke-Cheng Lu, Hong-Jie Wang, Xiao-Yi Dong, and Guang-Yin Zhang, "105-kW Peak-Power Double-Clad Fiber Laser",IEEE Photonics Technol. Lett. 15, 652 (2003).

68. M. Laroche, H. Gilles, S. Girard, N. Passilly, and K. Ait-Ameur, " Nanosecond Pulse Generation in a Passively Q-Switched Yb-Doped Fiber Laser by Cr^{4+}:YAG Saturable Absorber",IEEE Photonics Technol. Lett. 18, 764 (2006).